

(NASA-CR-124176) EVALUATION OF A 40 TO
 1 SCALE MODEL OF A LOW PRESSURE ENGINE
 (Lockheed Missiles and Space Co.) 106 p
 HC \$7.50 CSCL 21H

N73-21690

Unclas
 17046

G3/28

Lockheed

HUNTSVILLE RESEARCH & ENGINEERING CENTER

LOCKHEED MISSILES & SPACE COMPANY, INC.
 A SUBSIDIARY OF LOCKHEED AIRCRAFT CORPORATION

HUNTSVILLE, ALABAMA

LOCKHEED MISSILES & SPACE COMPANY INC.
HUNTSVILLE RESEARCH & ENGINEERING CENTER
HUNTSVILLE RESEARCH PARK
4800 BRADFORD DRIVE, HUNTSVILLE, ALABAMA

EVALUATION OF A 40:1
SCALE MODEL OF A LOW
PRESSURE ENGINE

31 December 1972

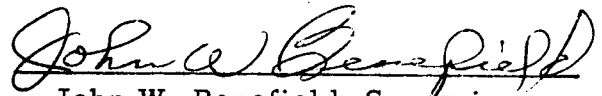
Contract NAS8-28899

Prepared for National Aeronautics and Space Administration
Marshall Space Flight Center, Alabama 35812

by

Charles E. Cooper
Jürgen Thoenes

APPROVED:



John W. Benefield, Supervisor
Fluid Mechanics Section



J. S. Farrior
Resident Director

FOREWORD

This report presents the results of work performed by Lockheed Missiles & Space Company, Inc., Huntsville Research & Engineering Center, under Contract NAS8-28899 for the NASA-George C. Marshall Space Flight Center, Marshall Space Flight Center, Alabama. The performance period covered by this final report is from 30 June through 31 December 1972. Mr. Charles S. Cornelius of the Control Mechanisms Branch of the Astrionics Laboratory's Guidance and Controls Division is the Technical Monitor for this contract.

CONTENTS

Section		Page
	FOREWORD	ii
	NOMENCLATURE	v
1	INTRODUCTION AND SUMMARY	1
2	TECHNICAL DISCUSSION	3
	2.1 Conceptual Background of Thrust Vector Control	3
	2.2 Scaling Parameters for TVC Studies	3
	2.3 Side-Force Prediction Techniques	12
	2.4 Gaseous Secondary Injection Side Force Calculations	14
3	ROCKET NOZZLE FLOW SIMULATION	23
	3.1 General	23
	3.2 TVC Facility Geometric Requirements	23
	3.3 TVC Test Facility Gasdynamic Simulation Requirements	24
4	GASEOUS TVC TEST FACILITY REQUIREMENTS AND CHARACTERISTICS	25
	4.1 General	25
	4.2 Facility Requirements	25
	4.3 Recommendations	27
	REFERENCES	29

Table

LIST OF TABLES

1	SITVC Mathematical Model	32
2	Basic Assumptions Used in LMSC Three-Dimensional JI Model	33
3	Basic Input/Output to LMSC Three-Dimensional Slot Jet Program	34

LIST OF TABLES (Continued)

Table		Page
4	Sensitivity to Input Parameters	35
5	Typical Booster Contoured Nozzle Coordinates	37

LIST OF ILLUSTRATIONS

Figure		
1	Component Diagram for Secondary Injection Thrust Vector Control Forces (Ref. 19)	38
2	TVC Side Force Ratio vs Secondary Mass Flow Ratio (X/L = 0.25)	39
3	TVC Side Force Ratio vs Secondary Mass Flow Ratio (X/L = 0.50)	40
4	TVC Side Force Ratio vs Secondary Mass Flow Ratio (X/L = 0.75)	41
5	TVC Nozzle Constant Mach Number Contours	42
6	Variation of the Ratio of Specific Heats for a Typical Booster Engine	43
7	Variation of the " ρu " Product at the Nozzle Exit Plane as a Function of Percent N ₂ in Mixture of CF ₄ /N ₂ and Chamber Temperature T _c (M _{primary} = 3.0)	44
8	Effect of Injection Angle on TVC System Performance (Refs. 20 and 21)	45
9	Effect of Multiple Orifices on TVC System Performance	46
10	Effect of Model Size on Test Facility Flow Rate and Operating Cost	47
11	Schematic of Thrust Vector Control Facility	48
12	TVC Test Facility Heater	49

Appendixes

A	Modeling the Three-Dimensional Effects of a Slot Jet Flow Field	A-1
B	User's Manual for the Thrust Vector Control Performance Program	B-1
C	Listing of the TVC Performance Computer Program	C-1
D	Non-Flow Through Pebble Bed Heater Performance	D-1

NOMENCLATURE

Symbol

A	geometric flow area
A_j	thrust vector control (TVC) system flow area
a_j	TVC system sonic velocity
AF	amplification factor
C^*	characteristic velocity
C_d	nozzle discharge coefficient
C_f	thrust coefficient associated with TVC operation
C_{f_v}	ideal vacuum thrust coefficient
C_{m_s}	secondary nozzle flow coefficient
d_t	TVC slot throat width
F_i	integrated pressure force
F_j	TVC thrust force
F_{jv}	TVC vacuum thrust
g	blast wave correction factor
h	TVC jet penetration parameter
I_{sp}	specific impulse
M	flow Mach number
m	massflow rate
P	pressure
P_j	TVC system static pressure
P_{o_j}	TVC system total pressure
R	radial distance to the nozzle wall measured from the nozzle axis

NOMENCLATURE (Continued)

Symbol

R_j	gas constant
S	primary nozzle interaction distance
T_{o_j}	TVC system total temperature
u	local flow velocity
v_t	local throat velocity
W	molecular weight
x	longitudinal distance along the nozzle axis measured from the throat

Greek

α	primary nozzle divergence half-angle
γ	ratio of specific heats
Γ	compressible flow parameter defined in Eq. (4) of Section 2.4
ϵ	secondary flow injection angle (see Fig. 2)
ν	blast wave coefficient calculated from Eq. (9) of Section 2.4
η_{n_s}	secondary nozzle thrust effectiveness
η	empirical spreading loss correction factor
ρ	density
ω	blast wave coefficient calculated from Eq. (10) of Section 2.4
ω_1	blast wave coefficient calculated from Eq. (11) of Section 2.4
ω_2	blast wave coefficient calculated from Eq. (12) of Section 2.4
ω_3	"weak wave" coefficient calculated from Eq. (14) of Section 2.4

NOMENCLATURE (Continued)

Subscripts

i	interaction force component
in	resultant interaction force
m	TVC parameter due to secondary injection momentum
n	normal momentum TVC parameter
P	primary nozzle parameter
s	secondary nozzle parameter
si	TVC side force component perpendicular to the primary nozzle axis
t	total pressure or temperature value
v	vacuum
x	component along the primary nozzle axis
y	component normal to the primary nozzle axis
1	interaction coefficient calculated from blast wave theory
2	interaction coefficient calculated from "weak wave" theory
*	parameter evaluated at total conditions
∞	local parameter value in the primary nozzle

Section I
INTRODUCTION AND SUMMARY

Space vehicles and missiles which have active guidance systems require a means of implementing control of the vehicle. This control function may be required over large ranges of velocity, acceleration, altitude and vehicle orientation (angles of attack, yaw and roll). There are four basic means for providing this control: (1) inertial systems such as those used on satellites in orbit; (2) reaction control systems (RCS) which utilize small thrusters; (3) aerodynamic control surfaces used in the sensible atmosphere; and (4) thrust vector control systems (TVC) which change the direction of the engine thrust vector. The means of control used on a vehicle is dictated by the flight regions in which it operates.

Future space vehicles will fly ascent and reentry trajectories which pass from the sensible atmosphere to near vacuum environment and return. These vehicles will therefore use a combination of aerodynamic surface controls, TVC or RCS. It is anticipated that the TVC system will be relied upon to provide launch vehicle stability and control over much of the flight trajectory. One type of TVC is secondary injection TVC.

The characteristics and performance of secondary injection thrust vector control (SITVC) systems are highly dependent upon the hardware characteristics used to implement the system, the injector geometry, nozzle injection locations, injection attitude, main nozzle characteristics, main propellants, and secondary injection fluid. Scale model tests of secondary injection systems can provide useful data for the evaluation of SITVC. However, depending upon the systems being modeled, significant variations in the degree of simulation can be encountered unless attention is given to the gasdynamic and kinetic scaling of the interacting flows.

The objective of this effort is to evaluate a scale model of a low-pressure rocket engine which is to be used for secondary injection studies. The following specific tasks were pursued under this contract:

1. Assess the test conditions which are required to achieve full-scale simulations. For scale model tests where full-scale simulation is not achieved, perform calculations to obtain estimates of the effects of non-simulation on SITVC performance.

2. Recommend fluids to be used for both primary and secondary flows, and suggest test operating conditions such as chamber pressures, injection pressure, injection velocity and other relevant parameters.

3. Recommend possible modifications to be made to the scale model and its test facility to achieve the highest possible degree of simulation.

This report presents a discussion of the theoretical and empirical scaling laws which must be observed to apply scale model test data to full-scale systems and describes a technique by which the side forces due to secondary injection can be analytically estimated.

Based on method-of-characteristics calculation for a typical full-scale nozzle and its scale model, recommendations are given with regard to scale model nozzle geometric and test fluid parameters which must be observed in order to suitably simulate the SITVC system effects. Also included is a critical evaluation of the scale model test facility being considered by MSFC.

Section 2 TECHNICAL DISCUSSION

2.1 CONCEPTUAL BACKGROUND OF THRUST VECTOR CONTROL

The concept of thrust vector control by secondary injection was conceived in 1949 by A. E. Wetherbee, Jr. (U. S. Patent 2,943,821), Ref. 1. Much research and development effort has been conducted in this area since 1952, and the concepts have been extended to cover supersonic mixing and combustion. Most of the investigations have been conducted for the case of a two-dimensional slot or round jet on the surface of a two-dimensional flat plate expanding into a uniform approach flow (Refs. 2 through 6). Ambient temperature air or inert gases were used in most of these studies. Although the results of these studies have been extremely important in the development of the TVC concept, they are limited to basic two-dimensional flow applications. Future applications necessitate that the TVC state of the art be extended to include an understanding of the jet interacting with complex, three-dimensional approach flow.

2.2 SCALING PARAMETERS FOR TVC STUDIES

The task of scaling the jet interaction phenomena has been practiced by many investigators as evidenced by the large number of reports on experimental studies. Although much knowledge has been gained by these works and the techniques for scaling the jet interaction phenomena are well established, it is often difficult to duplicate the scaling parameters from a practical aspect. Therefore it is of the utmost importance to examine the scaling techniques that have been used in the past and evaluate them in terms of future applications.

As stated previously, the jet interaction phenomena as defined for this program are composed of the complex interactions of a sonic jet expanding

from the nozzle wall with the supersonic main flow surrounding the secondary jet. Scaling these phenomena for a prototype engine involves scaling the engine nozzle and secondary jet nozzle geometry, considering the properties of jet working fluid, and gas dynamic characteristics of jet and main nozzle flows.

Geometric scaling of the prototype engine is an accepted practice for model tests and is of particular importance in terms of the jet interaction effects. The relative size, location and orientation of the jet port on the prototype must be maintained on the model. This is to ensure that scaled jet plume interaction with adjacent surfaces will be possible, assuming that the correct gas dynamic simulation of the jet has been achieved. Therefore, in a parametric study of the jet interaction effects, the sensitivity to jet size, location and orientation should be investigated.

In gasdynamic scaling of rocket engine flows, matching of the Reynolds number is an accepted criterion. Recalling the definition of Reynolds number as $\rho uL/\mu$, it can be shown that for a geometrically scaled model, using the full-scale gas, the Reynolds number of the flow in a nozzle can be matched only if the density, ρ , is increased via a chamber pressure (P_c) increase as the model scale is decreased. (For a one-tenth scale model, a chamber pressure equal to ten times full scale is required to match full-scale Reynolds number.) If the required Reynolds matching can be achieved the resulting test data should give full-scale results (presuming full-scale operating fluids are used).

Relating the above information to SITVC studies, it becomes immediately apparent that the Reynolds numbers of both the injector flow and of the flow in the primary nozzle should match full-scale values. It is determined rather quickly, however, that the above conditions are not practiced for most test programs. The magnitude of the pressure levels required to obtain full-scale Reynolds number in scale model TVC programs are, in general, beyond the practicalities of existing test facilities. It is also quickly determined that the use of the full-scale gases may be impossible or impractical due to handling problems or the difficulty of duplicating the combustion products at a reasonable cost.

Accepting the fact that full-scale Reynolds numbers of the primary and injector nozzle flows cannot be matched, the next most desirable condition is that which would minimize the effects of Reynolds number. This condition is generally accepted to exist when the local Reynolds number is of sufficient magnitude such that the flow adjacent to the body is turbulent; i.e., the local Reynolds number is greater than or equal to 10^6 .

Methods for determining boundary layer transition is a separate study and will not be discussed here; however, previous analysis of large rocket engines has confirmed that the flow in the region of the TVC injection ports is fully turbulent. The following discussions of the problem of simulating the full-scale system will be predicated on the assumption of the model operating in the turbulent flow regime.

From the preceding discussion it becomes immediately apparent that "direct" scaling cannot be achieved in most TVC test programs. A "simulation" technique must therefore be employed where the effects of Reynolds number are considered to be second order and negligible. This results in the dilemma faced in most TVC model testing — what parameters must be considered to "simulate" the full-scale conditions and how does one accomplish the simulation?

In general, it is extremely difficult to simultaneously simulate (theoretically or experimentally) both the inviscid and viscous aspects of the gas dynamics. In some instances simulation of only the inviscid characteristics has been all that is required to obtain meaningful results. It is anticipated that meaningful simulation of the flow phenomena to obtain TVC pressure information will require consideration of both inviscid and viscous effects. The simulation of these effects is discussed in the paragraphs that follow.

The complexity of the TVC flow problem has obstructed the development of a general analytical solution and increased the need for developing experimental techniques. To obtain meaningful experimental results, the full-scale flow field must be simulated. The parameters required for similitude must,

therefore, be identified and substantiated through experiment. Two phenomena associated with TVC performance which should be simulated are the penetration depth and the plume shape resulting from secondary injection into the primary flow.

The penetration of the injector flow into the primary stream is essentially one case of the expansion of a sonic or supersonic jet into a nonquiescent stream. It would therefore seem logical that simulation parameters evolved for similar problems might also be applicable to the TVC problem. Goethert and Barnes (Ref. 7) addressed the problem of simulation of base flow phenomena with a cold gas. They showed that for simulation of a supersonic jet expanding into a parallel supersonic flow, the following inviscid parameters should be satisfied:

- Geometric scaling of the nozzle
- $$\left(\frac{\gamma_j M_j^2}{\sqrt{M^2 - 1}} \right)_{\text{model}} = \left(\frac{\gamma_j M_j^2}{\sqrt{M_j^2 - 1}} \right)_{\text{prototype}}$$
- $$\left(\frac{P_j}{P_\infty} \right)_{\text{model}} = \left(\frac{P_j}{P_\infty} \right)_{\text{prototype}}$$
- $$\left(\frac{\gamma P M^2)_j}{\gamma P M^2)_\infty} \right)_{\text{model}} = \left(\frac{\gamma P M^2)_j}{\gamma P M^2)_\infty} \right)_{\text{prototype}}$$

Satisfactorily matching these parameters results in the matching of the shape of the full-scale inviscid plume boundary. In order to match not only the inviscid plume boundary, but also the detailed inviscid flow structure (which is necessary for achieving correct inviscid force ratios) then it is also mandatory to have the correct values of γ_j and γ_∞ . For the case of the TVC studies, matching these parameters should result in the correct inviscid relationship between injector and primary flows.

Since the basic nature of the interaction of a jet with an external flow involves viscous effects and the mixing process, the relations which describe these phenomena were reviewed to establish conditions for viscous similitude between

the full-scale and model flows. To determine a "viscous mixing" similarity parameter, empirical eddy viscosity models of several types were applied to the momentum equation for steady, compressible flow (Ref. 8). The models used and the resultant similarity parameters are summarized below:

Schetzian Model 3

$$\frac{\left. \frac{\rho_j u_j}{\rho_\infty u_\infty} \right|_M}{\left. \frac{\rho_j u_j}{\rho_\infty u_\infty} \right|_{FS}} = 1$$

Donaldson and Gray

$$\frac{\left. \frac{u_\infty}{u_j} \right|_M}{\left. \frac{u_\infty}{u_j} \right|_{FS}} = 1 \quad \text{and} \quad \begin{aligned} M_{jM} &= M_{jFS} \\ M_{\infty M} &= M_{\infty FS} \end{aligned}$$

Schetzian Unified Theory

$$\frac{\left. \frac{\rho_\infty u_\infty}{\rho_j u_j} \right|_{FS}}{\left. \frac{\rho_\infty u_\infty}{\rho_j u_j} \right|_M} = 1$$

Based on the results of Ref. 8 it was concluded that matching of the ratio of the " ρu " product for injectant and primary flows between prototype and model

is an apparent similarity parameter for TVC flow simulation. A systematic parametric test program will be required to establish the ρu ratio as a similarity parameter.

The " ρu " ratio parameter can be rewritten in the following form using the equation of state and the definition of sonic velocity:

$$\left. \frac{\rho_{\infty} u_{\infty}}{\rho_j u_j} \right|_{FS} = \frac{\left. \frac{\gamma PM}{(\gamma RT)^{1/2}} \right|_{\infty}}{\left. \frac{\gamma PM}{(\gamma RT)^{1/2}} \right|_j} \Bigg|_{FS} = \frac{\left. \frac{\gamma PM}{(\gamma RT)^{1/2}} \right|_{\infty}}{\left. \frac{\gamma PM}{(\gamma RT)^{1/2}} \right|_j} \Bigg|_M = \left. \frac{\rho_{\infty} u_{\infty}}{\rho_j u_j} \right|_M$$

An examination of this expression reveals that the " ρu " ratio parameter imposes an additional requirement on the ratio of the sonic velocity of the injectant and primary gases. Rearranging the above expression and assuming that the " γPM " ratio for prototype and model are equal (i.e.,

$$\gamma_{j_{\text{model}}} = \gamma_{j_{\text{full scale}}} ; M_{j_{\text{model}}} = M_{j_{\text{full scale}}} ; \left. \frac{P_j}{P_{\infty}} \right|_{\text{model}} = \left. \frac{P_j}{P_{\infty}} \right|_{\text{full scale}} ;$$

$$\gamma_{\infty_{\text{full scale}}} = \gamma_{\infty_{\text{model}}} ; \text{ and } M_{\infty_{\text{full scale}}} = M_{\infty_{\text{model}}}), \text{ then}$$

$$\left. \frac{(\gamma RT)_j^{1/2}}{(\gamma RT)_{\infty}^{1/2}} \right|_{FS} = \left. \frac{(\gamma RT)_j^{1/2}}{(\gamma RT)_{\infty}^{1/2}} \right|_M$$

Therefore

$$\left. \frac{a_j}{a_{\infty}} \right|_{FS} = \left. \frac{a_j}{a_{\infty}} \right|_M$$

Therefore, in summary, an examination of the requirements for gas-dynamic similitude of full-scale and model flows has resulted in the following similarity conditions:

- Geometry – full-scale primary and injector nozzle contour geometry properly scaled.
- Gasdynamic scaling

$$\text{(Inviscid)} \quad \left. \frac{\gamma_j P_j M_j^2}{\gamma_\infty P_\infty M_\infty^2} \right|_M = \left. \frac{\gamma_j P_j M_j^2}{\gamma_\infty P_\infty M_\infty^2} \right|_{FS}$$

where

$$\gamma_{\infty M} = \gamma_{\infty FS}; \gamma_{jM} = \gamma_{jFS}; M_{\infty M} = M_{\infty FS};$$

$$M_{jM} = M_{jFS}; \text{ and } \left. \frac{P_j}{P_\infty} \right|_M = \left. \frac{P_j}{P_\infty} \right|_{FS}$$

$$\text{(Viscous)} \quad \rho u \Big|_M \equiv \frac{\rho_\infty u_\infty}{\rho_j u_j} \Big|_M = \frac{\rho_\infty u_\infty}{\rho_j u_j} \Big|_{FS} \equiv \rho u \Big|_{FS}$$

These parameters can be readily satisfied if gamma (γ_j) of the model jet is equal to γ_j of the prototype. If γ_j 's are not equal, then adjustments must be made in nozzle geometry to change the model area ratio and ultimately the jet chamber pressure. The parameters P_j/P_∞ and $\gamma PM^2)_j/\gamma PM^2)_\infty$ have been used in Refs. 10 and 11, respectively, to correlate analytical and experimental jet interaction data. Inherent in the above parameters is the requirement that the primary nozzle flow conditions be the same for model and prototype.

By appropriately combining the above equations Zukoski and Spaid (Ref. 12) have determined a scaling parameter convenient for TVC applications.

This scaling parameter can be stated as

$$\left[\frac{\dot{m}_j [T_{o_j}/W_j]^{1/2}}{\dot{m}_\infty [T_{o_\infty}/W_\infty]^{1/2}} \right]_{\text{prototype}} = \left[\frac{\dot{m}_j [T_{o_j}/W_j]^{1/2}}{\dot{m}_\infty [T_{o_\infty}/W_\infty]^{1/2}} \right]_{\text{model}}$$

The appearance of total temperature, T_o , and molecular weight, W , introduces additional complications. In addition to satisfying the above relationship, the jet nozzle must be geometrically scaled, and the ratio of jet to free stream total pressure (P_{o_j}/P_{o_∞}) must be maintained to ensure no scaling errors.

Correlation of interference pressure data for different pressure ratios and nozzle diameters for an underexpanded jet in a supersonic flow was obtained by using a length parameter, h , in Ref. 13. This parameter denotes the distance from the nozzle exit to the Mach disk or to the first intersection of the "diamond" shock pattern when this configuration exists. The parameter "h" is defined by the empirical equation:

$$\frac{h}{d_j} = 0.645 \left[\frac{P_{o_j}}{P_\infty} \right]^{1/2}$$

For correlation purposes d_j is replaced by d_t , jet nozzle throat diameter. For conditions where the exit Mach number of the model and prototype jet nozzle are the same, the above equation can be applied to scale the jet interaction phenomena. Examination and manipulation of these correlation/scaling parameters can show that they are inherently included in the gasdynamic scaling parameters summarized on page 9.

Therefore, the requirements which must be met in order to accurately simulate the secondary injection phenomena for a non-reacting system can be summarized as follows:

- Scale Geometry
- Jet characteristics - P_{o_j} , T_{o_j} , γ_j , M_j , W_j
- Engine gas dynamic characteristics - P_{o_∞} , T_{o_∞} , γ_∞ , M_∞ , W_∞
- Gasdynamic scaling parameters

$$\frac{P_j}{P_\infty} ; \frac{\gamma PM^2)_j}{\gamma PM^2)_\infty} ; \frac{\rho_j u_j}{\rho_\infty u_\infty} \left(\text{i.e., } \frac{\gamma PM_j}{\gamma PM_\infty} \right)$$

and that some useful side force correlation parameters are:

$$\frac{\dot{m}_j \left[T_{o_j} / W_j \right]^{1/2}}{\dot{m}_\infty \left[T_{o_\infty} / W_\infty \right]^{1/2}} ; \frac{h}{d_j}$$

The sensitivity of the scaling of the jet interaction phenomena to variations in the basic gasdynamic parameters is not known. The applicability of scaling parameters evolved from simple two-dimensional models is also in question. Therefore, without any obvious optimum choice, scaling of jet interaction phenomena for this study will be based on the similarity parameters which have been used to simulate the plume of an underexpanded jet exhausting to a supersonic flow. In addition, investigators have reported dependency of jet interference on the injectant molecular weight and total temperature (Refs. 14 and 15). Therefore, the sensitivity of the jet interaction phenomena to variations in the following gasdynamic parameters should be investigated:

- Jet exit to engine flow static pressure ratio, P_j/P_∞
- Jet exit Mach number, M_j

- Jet exit gamma, γ_j
- Jet exit molecular weight, W_j
- Jet total temperature, T_{o_j}
- Engine flow approach conditions, M_∞, P_∞

In the process of conducting the tests in which the above gasdynamic parameters are used as independent variables, the effects of the scaling relations will also be obtained. By selecting the proper test fluids, each of the above gasdynamic parameters can be varied independently during the course of a parametric study.

2.3 SIDE-FORCE PREDICTION TECHNIQUES

The phenomenon of a secondary jet expanding perpendicularly into a supersonic mainstream has been described and documented by various investigators, for example Refs. 12, 13, 16, 17 and 18. The generally accepted major features of this phenomenon are schematically defined in Fig. 1 of the Appendix. The turning of the nozzle flow due to interaction with the secondary jet substantially raises the pressure (P_2) on the surface of the nozzle wall upstream and immediately around the jet port(s). The integrated effect of these pressure increases over the separated flow region augments the pure reaction force of the jet. The ratio of the sum of this integrated pressure force (F_i) and the TVC motor thrust normal to the engine surface at the point of injection to the jet motor vacuum thrust (F_{jv}) defines the TVC force amplification factor, AF, as follows:

$$AF = \frac{F_y/F_x}{\dot{m}_s/\dot{m}_p}$$

At realistic conditions with the main engine firing, the amplification factor can increase up to approximately four, depending upon the approach flow properties, secondary jet gas properties and nozzle geometry.

The jet interaction phenomenon has been mathematically modeled by many investigators. A summary of some of the more pertinent models is shown in Table 1. These models are, in general, limited to two-dimensional or modified two-dimensional flow situations and are not applicable to problems associated with the flow in contoured rocket nozzles which is three-dimensional.

The development of a three-dimensional slot jet mathematical model which addresses some of the problems associated with TVC application was accomplished in a Lockheed Independent Development Study during 1969 and 1970. This model, which is capable of estimating supersonic boundary layer jet interaction control force characteristics, has been coded for application to digital computers and is available for engineering studies. A brief discussion of this model is presented in the following paragraphs. A more detailed description of the development of this model is included in the Appendix of this document.

The three-dimensional gas interaction mathematical model, Fig. 4 of the Appendix, is based upon a momentum balance. It consists of equating the drag on the slot plume (equivalent) to the change in axial momentum of the transverse jet. The basic assumptions used in formulating this model are summarized in Table 2. The mean reattachment pressure on the upstream face of the injected plume and the base pressure on the downstream side, in the present computer program, are computed using Spaid and Zukoski's empirical constants (Ref. 4). However, if desired, the downstream empirical constant can be computed by using the method proposed by Maurer (Ref. 5) to handle the effects of slot inclination angle while the upstream empirical constant may be related to the mixing theory proposed by Korst (Ref. 18). Flow which turns around the end of the slot and proceeds downstream is assumed

to have a boundary layer separation pressure value over a quarter circle area* with a radius equal to the computed separation distance at the end of the slot span. The end effect significantly increases the boundary layer separation force produced by the jet interaction phenomena. The magnitude of the ratio, boundary layer separation force to jet reaction force, is a function of: local freestream Mach number, slot aspect ratio, injected gas total to freestream static pressure ratio, nozzle geometry, the direction of nozzle inclination, and the gas properties associated with the two streams. The Lockheed program will compute the penetration height of the injected gas and the point of freestream flow separation in front of the slot as a result of three-dimensional flow over and around a transverse jet injected into a freestream flow field. Although the above is applicable for a flat plate, the incremental force terms can be warped to account for body curvature within the existing computer program.

The INPUT and OUTPUT parameters available in the Lockheed program are presented in Table 3. The sensitivity of the amplification factors to program input parameters is discussed in Table 4.

2.4 GASEOUS SECONDARY INJECTION SIDE FORCE CALCULATIONS

The procedure presented in this section for calculating thrust vector control performance was developed by personnel of the Aerotherm Corporation (Ref. 19) as a part of Air Force Programs AFO4(611)-9075 and AF04(611)-9960. The technique appears to be applicable to predict both liquid and solid motor TVC system performance as shown by the data comparisons in Dahm's report (Ref. 19)

* A blast wave solution has also been programmed and checked out on the computer; however, further comparisons with test data are needed to verify its accuracy. For this reason and since the above theory applies to slot injection the approach of Section 2.4 will be used.

The basic approach for developing a suitable calculational technique is first to determine the nature of the components which make up the TVC side force, then to arrive at equations which describe these forces, and finally to ascertain how these forces make themselves felt in the form of vehicle turning moment. The subsequent paragraphs describe each of these items in detail.

The injection of a non-reacting gas into the supersonic exhaust flow of a rocket nozzle is a means to generate lateral force on the nozzle with a resulting turning moment to provide pitch control for the vehicle. The lateral force is a result of the contributions of the momentum thrust of the injection flow and the interaction forces due to the separation of the primary nozzle flow by the secondary flow. Figure 1 presents a component diagram of these TVC forces (single port injection).

The equations to calculate the magnitude of the TVC forces are in part based on the following assumptions:

- a. The state of the primary gas may be calculated using real or ideal gas thermochemistry. These calculations will be made using a recognized technique e.g., the method of characteristics.
- b. Flow within the secondary injection port is assumed to be described adequately by a one-dimensional analysis. The secondary nozzle is also assumed to be circular at its exit with the flow considered to be adiabatic.

The forces due to the momentum of the secondary jet are composed of forces acting parallel to the secondary nozzle centerline (F_m) and normal to the secondary nozzle centerline (F_{mn}).

The basic one-dimensional momentum equation describing the thrust generated parallel to the secondary nozzle axis is:

$$F_m = \eta_{n_s} (\rho'_s A'_s u'^s_2 + p_s A_s)_{ideal} - \rho_\infty A_s \quad (1)$$

where the primed parameters refer to the one-dimensional value of these parameters at the secondary nozzle exit and η_{n_s} is the secondary nozzle thrust efficiency. The value of η_{n_s} accounts for the thrust losses due to surface shear forces, non one-dimensionality and real gas effects. Dividing all terms in Eq. (1) by the actual "corrected" mass flow rate, $m_s C_s^*$ one arrives at a form of the equation which is more convenient for TVC calculations

$$C_{f_m} = \eta_{n_s} C_{f_v} - \frac{p_\infty}{p_{tP}} \left(\frac{m_p C_p^*}{m_s C_s^*} \right) \frac{A_s}{C_{dp} A_p^*} \quad (2)$$

where C_{f_v} comes from the following equation

$$C_{f_v} = \frac{\Gamma (1 + \gamma M_s^2)}{\gamma^{1/2} M_s \left(1 + \frac{\gamma-1}{2} M_s^2\right)^{1/2}} \quad (3)$$

and

$$\Gamma = \gamma^{1/2} \left(\frac{2}{\gamma+1} \right)^{\frac{\gamma+1}{2(\gamma-1)}} \quad (4)$$

and

$$C^* = \frac{\sqrt{R T_t}}{\Gamma} \quad (5)$$

Equation (2) is valid when the value of the secondary exit stagnation pressure is sufficiently high to ensure sonic or supersonic flow at the secondary nozzle exit.

The normal component of the momentum thrust F_{m_n} is developed from the following basic relation

$$F_{m_n} = p_s A_s \left(\frac{\pi}{2} - \frac{\epsilon \pi}{180} \right) - p_\infty A_s \cot \epsilon \quad (6)$$

where ϵ is the injection angle (Fig. 1) measured in degrees.

Dividing Eq. (6) by the secondary "corrected" mass flow and employing basic gasdynamic relationships one obtains the following equation describing the normal momentum thrust coefficient

$$C_{f_{m_n}} = \frac{\pi \Gamma_s \left(\frac{1}{2} - \frac{\epsilon}{180} \right)}{C_{m_s} \gamma^{1/2} M_s \left(1 + \frac{\gamma_s - 1}{2} M_s^2 \right)^{1/2}} - \frac{p_\infty}{P_{t_p}} \left(\frac{m_p C_p^*}{m_s C_s^*} \right) \frac{A_s}{C_{d_p} A_p^*} \cot \epsilon \quad (7)$$

The forces due to the interaction of the secondary jet with the primary fluid are spread in a multiplicity of directions. The resultant force, however, may be described as a force acting normal to the primary nozzle wall, F_{in} . Work performed by Aerotherm personnel (Ref. 19) has shown that the "blast wave" theory of Sakauri (Refs. 20 and 21) is valid for a range of "moderately high" secondary mass flow rates but that poor agreement with test data was noted for the "low" secondary mass flow rates. The work also showed that for "low" injection rates the results of Walker and Shandor (Ref. 22) adequately predicted the low flow rate regime.

The interaction thrust coefficient applicable to the high mass flow rate situation is derived in Ref. 19 and is herein referred to as Theory 1.

The interaction thrust coefficient generated by Theory 1 is given by

$$C_{f, in_1} = g\nu\omega \left(\frac{S}{C_{dp}^{1/2} d_p^*} \right)^{1/2} \left(\frac{\dot{m}_p C_p^*}{\dot{m}_s C_s^*} \right)^{1/4} \quad (8)$$

where g is an empirically determined correction factor to account for the difference between the injection Mach number and the hypersonic Mach number for which the blast wave theory was developed. For the freestream Mach number range of interest g has been found to be essentially constant, ($g = 0.7$, Ref. 23).

As shown by Dahm (Ref. 24) the value of ν is calculated from

$$\nu = 1.175 \gamma_p - 1.05 \quad (9)$$

ω is calculated from

$$\omega = \omega_1 (\omega_2)^{3/4} \quad (10)$$

where

$$\omega_1 = \frac{M_\infty^{3/4}}{\left(1 + \frac{\gamma_p - 1}{2} M_\infty^2 \right)^{\frac{5\gamma_p - 3}{8\gamma_p - 3}}} \left(\frac{C_p^*}{C_s^*} \right) \quad (11)$$

and

$$\omega_2 = 1/2 + \frac{1}{\gamma_p(\gamma_p-1) M_\infty^2} + \frac{\gamma_s}{\gamma_s-1} \frac{1 + \frac{\gamma_p-1}{2} M_\infty^2}{\gamma_p M_\infty^2} \left(\frac{\Gamma_s}{\Gamma_p}\right)^2 \left(\frac{C_s^*}{C_p^*}\right)^2 \quad (12)$$

$$+ \frac{M_s}{M_\infty} \left(\frac{1 + \frac{\gamma_p-1}{2} M_\infty^2}{1 + \frac{\gamma_s-1}{2} M_s^2}\right)^{1/2} \left(\frac{\gamma_s^{1/2} \Gamma_s}{\gamma_p^{1/2} \Gamma_p}\right) \frac{C_s^*}{C_p^*} \cos \epsilon$$

The authors of Ref. 22 have developed a theory (referred to as theory 2) to describe the low secondary mass flow rate situation by coupling two-dimensional linearized supersonic flow theory with the one-dimensional flow theory influence coefficients to obtain the resulting expression

$$C_{f, in2} = \frac{\gamma_p^{1/2} \Gamma_p (\gamma_p - 1) M_\infty^3}{\left[(M_\infty^2 - 1) \left(1 + \frac{\gamma_p-1}{2} M_\infty^2\right)\right]^{1/2}} \left(\frac{C_p^*}{C_s^*}\right) \omega_3 \quad (13)$$

where

$$\omega_3 = \omega_2 + \frac{1}{(\gamma_p-1) M_\infty^2} \left\{ \frac{W_p}{W_s} \left[1 - \frac{\gamma_s}{\gamma_p} \left(\frac{\gamma_p-1}{\gamma_s-1}\right) \right] + \frac{\gamma_p-1}{\gamma_p} \right. \quad (14)$$

$$\left. + \frac{M_s}{M_p} \left(\frac{1 + \frac{\gamma_p-1}{2} M_\infty^2}{1 + \frac{\gamma_s-1}{2} M_s^2}\right)^{1/2} \left(\frac{\gamma_s^{1/2} \Gamma_s}{\gamma_p^{1/2} \Gamma_p}\right) \frac{C_s^*}{C_p^*} \cos \epsilon \right\}$$

To determine the range of applicability of Eqs. (8) and (13), Dahm recommends that one should perform both calculations and conservatively choose the smaller value of the interaction force coefficient.

The only remaining item to consider is the reduction in the calculated interaction forces due to the circumferential spreading loss. This empirically determined factor is necessary to account for the observed overprediction of side forces by both theories 1 and 2. Dahm shows that the factor (η_ϕ) is reasonably well described by

$$\eta_\phi = 1 - 0.65 \left(\frac{S}{d_{ep}} \right)^{3/4} \quad (15)$$

For lack of better data, η_ϕ has been assumed to vary with geometry only, independent of secondary mass flow rate.

The previously calculated momentum force coefficients may be resolved into components acting parallel (C_{m_x}) and perpendicular (C_{m_y}) to the primary nozzle centerline, as follows

$$C_{m_x} = -C_m \cos(\alpha + \epsilon) + C_{mn} \sin(\alpha + \epsilon) \quad (16)$$

$$C_{m_y} = C_m \sin(\alpha + \epsilon) + C_{mn} \cos(\alpha + \epsilon) \quad (17)$$

The forces due to the interaction effect may be characterized by a single force acting normal to the primary nozzle wall. Resolving this force into the same x and y coordinate system as used in the momentum case, one arrives at

$$C_{ix} = C_{in} \sin \alpha \quad (18)$$

$$C_{iy} = C_{in} \eta_{\phi} \cos \alpha \quad (19)$$

The final effect of the secondary gas injection may be calculated by combining the components computed by Eqs. (15) through (18) with the result

$$\Delta C_x = C_{mx} + C_{ix} \quad (20)$$

$$C_y = C_{my} + C_{iy} \quad (21)$$

and the common performance parameter, i.e., the amplification factor (AF) obtained from the following relation

$$AF = \frac{F_y/F_x}{m_s/m_p} = \left(\frac{C_y m_s C_s^*}{C_{fp} m_p C_p^* + \Delta C_x m_s C_s^*} \right) \frac{m_p}{m_s}$$

Figures 2, 3, and 4 show the results of sample calculations for a typical secondary injection TVC system. The conditions simulated are: isentropic exponent $\gamma_p = \gamma_s = 1.15$, secondary injection Mach number = 1.0, primary nozzle chamber pressure = 700 psia, primary nozzle area ratio = 7.0, and the primary nozzle divergence half-angle = 17.5 degrees.

The following parameters were varied

- Secondary mass flow ratio was varied considering a fixed secondary injection area with a varying secondary injection pressure.
- Secondary injection angle was varied from 15 to 75 degrees away from the primary nozzle wall.
- The axial injection location was varied from $x/L = 0.25$ to $x/L = 0.75$.

The calculated data indicate the advantage one gains from injecting gas in an upstream direction and also show that moving the injection point downstream is advantageous. However, the data at the extreme downstream location are questionable due to the incompleteness of the blast wave theory (see Ref. 19, p. 2-9).

Section 3

ROCKET NOZZLE FLOW SIMULATION

3.1 GENERAL

Future space vehicles presently being investigated will be expected to operate from a near vacuum environment through the region of high reentry pressures and angles of attack to subsonic flight. To maintain the stability and control characteristics of the vehicle over this large range of conditions TVC systems and aerodynamic surfaces may be used.

To design a TVC system capable of meeting these requirements one must determine from analytical and empirical means the physical characteristics such a TVC system must possess. Section 2 describes some of the accepted analytical techniques in use while this section will be devoted to the requirements necessary to obtain an adequate TVC test simulation and the relationship of these requirements to the proposed MSFC test facility. Logically this can be separated into a consideration of the (interrelated) test facility geometric aspects and the gasdynamic aspects of the test facility.

3.2 TVC FACILITY GEOMETRIC REQUIREMENTS

The primary aerodynamic phenomenon that governs the performance of a gaseous injection TVC system is the location and strength of the separated flow region generated by injecting a gas into the primary nozzle stream. The most important factor pertaining to the strength of the separation region is the local Mach number at which the separation occurs. One of the two most important parameters affecting the nozzle Mach number distribution is the nozzle contour. A typical set of full-scale booster engine contoured nozzle coordinates corresponding to a LOX/RP-1 propellant combination is presented in Table 5. Using the method of characteristics with real gas chemistry effects

accounted for, calculations were performed on this nozzle for a chamber pressure of $17.237 \times 10^5 \text{ N/m}^2$ (250 psia) and an oxidizer-to-fuel ratio of 2.8 with the resulting internal nozzle Mach number contours being given in Fig. 5. Superimposed on these results are the Mach number values obtained when method-of-characteristics calculations were made on the proposed 15-degree conical nozzle using cold air as the working medium. These results show that an adequate simulation of the nozzle internal Mach number distribution in the region of TVC injection cannot be obtained by using a conical nozzle to simulate a contoured bell nozzle. Thereafter, it is recommended that a scaled contour corresponding to the contour of Table 5 be employed for the MSFC TVC test facility.

3.3 TVC TEST FACILITY GASDYNAMIC SIMULATION REQUIREMENTS

In addition to accurately scaling the flight engine geometric characteristics, it is necessary to closely duplicate the value of the engine propellant ratio of specific heats, γ , as this parameter is fundamental to compressible flow calculations. Figure 6 shows a plot of the γ distribution using LOX/RP-1 that would occur along the wall of the contoured nozzle of Table 5 and the value of the constant γ resulting from using cold air as the test medium. Figure 6 also shows values of γ obtained by using a heated variable γ simulant gas. In this case carbon tetrafluoride (CF_4) was selected because it exhibits the desired low value of γ and has good handling characteristics, e.g., low toxicity, non-corrosiveness, etc. Figures 5 and 6 show that it is possible to obtain a reasonable simulation of the rocket nozzle internal Mach number characteristics by duplicating the nozzle contours and selecting a simulant gas whose ratio of specific heats is close to the ratio of specific heats of the full-scale engine propellants.* Figure 7 (Ref. 9) shows the variation of the ρu product as a function of CF_4/N_2 mixture ratio for a typical case.

* CF_4 is commercially available from several companies (DuPont, Matheson, etc.) and costs about \$7.70 per pound.

Section 4

GASEOUS TVC TEST FACILITY REQUIREMENTS
AND CHARACTERISTICS

4.1 GENERAL

This section discusses the mechanical requirements necessary to fabricate a test facility that will yield pertinent TVC system test data. Suggestions regarding the size and materials used for the facility are also given.

4.2 FACILITY REQUIREMENTS

To generate meaningful TVC system test data, as previously discussed in Section 3.3, it will be necessary to closely approximate the value of the ratio of specific heats of the main engine exhaust gas and the TVC system injectant gas. Since the propellant combinations for future space vehicles are subject to change it is recommended that a means of mixing gases to obtain a suitable γ be incorporated into the test facility design and that a means for heating the primary and injectant gases be provided. By a combination of mixed gases heated to the proper temperature, one can very nearly duplicate the γ value of virtually any propellant.

Previous test programs investigating gaseous TVC system characteristics have shown that the performance of the TVC system is strongly dependent upon the angle at which the TVC gas is injected into the primary stream. Figure 8 (Refs. 26 and 27) presents a typical set of TVC system performance data and shows that the level of the side force generated per pound of injectant gas is maximum when the injectant gas is inserted at an angle of approximately 30 degrees upstream. Therefore, it is recommended that rather than inject the gas normal to the nozzle centerline, it be injected in an upstream direction at an angle of about 30 degrees. It has also been demonstrated that

TVC system performance can be significantly improved by injecting the gas through multiple small orifices rather than a few large orifices. Figure 9 (Refs. 27 and 28) shows that increases in the TVC system I_{sp} from 40 to 80% may be anticipated by utilizing multiple orifices.

When initial consideration was given by MSFC personnel to building a TVC system test facility it was tentatively decided to construct it to accommodate a 40:1 scale model of a typical large booster engine and be capable of simulating engine thrust chamber pressure levels from $17.237 \times 10^5 \text{ N/m}^2$ (250 psia) to $117.21 \times 10^6 \text{ N/m}^2$ (1700 psia). While there is no question that such a facility could generate much useful information, further investigation disclosed that the capability of the MSFC high pressure air system was unable to supply sufficient mass flow to maintain supersonic flow in the nozzle at pressures above $41.37 \times 10^5 \text{ N/m}^2$ (600 psia). For this reason and because the test facility fabrication and operating costs would be reduced it is recommended that the model scale be decreased. Figure 10 shows the mass flow rate and propellant consumption cost as a function of model size. A throat radius of approximately 0.635 cm is suggested as this is still relatively easy to manufacture and would still provide meaningful test data to assess the TVC system performance although difficulties may be encountered due to the small injection port size. Also with regard to model costs it is suggested that consideration be given to fabricating the nozzle assembly from material that can be machined easier than the proposed stainless steel. Aluminum or a filled epoxy type of material such as Stycast would be suitable. Also, it is recommended that the test nozzle be rotatable around its longitudinal axis. This would allow the injectant scheme to be modified and would preclude fabricating a new nozzle.

Due to the relatively high temperatures and pressures at which the testing would be conducted it is recommended that all measurements and all position settings for movable parts such as valves be remotely controllable. Also, in order to avert the possible destruction of the test facility in the event of a major malfunction it is recommended that a restraining device be provided to limit the swiveling of the nozzle.

The final observation regarding the TVC test facility is that due to the high exit Mach number of the primary nozzle the noise level of the facility may be objectionable, necessitating that it be operated only at night.

4.3 RECOMMENDATIONS

In summary, the following suggestions and observations are made regarding the MSFC proposed test facility:

- A means of mixing gases and heating the mixture should be provided in both the primary and secondary flow circuits to obtain a suitable gamma for testing.
- The TVC fluid injection angle should be pointed upstream at an angle of approximately 30 degrees.
- A capability for injecting the TVC fluid through multiple small orifices rather than one large orifice is desirable.
- The test facility scale size should be reduced to a throat radius of approximately 0.635 cm.
- Fabricating the nozzle out of aluminum or a filled epoxy material should be considered.
- Making provision for rotating the nozzle on its mounting block will give added versatility.
- Provisions should be made so that all measurements and control can be remotely monitored and controlled.
- A safety ring should be provided to limit total nozzle travel. Testing may have to be conducted at night due to possible objectionable noise levels.

Figure 11 schematically shows a facility capable of generating TVC scale model test data with the foregoing suggestions incorporated where appropriate. It should be noted that the suggested facility is a "blowdown" rig in which provision has been made to mix in predetermined proportions a low gamma gas from high pressure bottles with MSFC supplied air in an independent plenum-heater arrangement. After the gases are bled into the plenums the isolation valves shown on Fig. 11 are closed and a suitable amount of time is allowed to ensure complete mixing of the gases. After mixing has taken place, the gases will be heated to the proper temperature to obtain the desired gamma at which time the downstream pressure regulators will be opened and a test run made.

Further explanation regarding the facility's operating characteristics will now be given. Figure 12 shows two possible ways of preparing the test gas to obtain the desired operating conditions ($P_c = 250$ psia, $T_T = 600^\circ\text{F}$). Concept 1 consists of a high pressure reservoir containing alumina (Al_2O_3) pebbles. These pebbles have sufficient thermal capacitance and a high enough convective heat transfer coefficient to maintain a constant exit temperature of the gas. The pebbles are heated in some manner (blowing heated air through the system, calrod units, etc.) to the desired test temperature at which time the simulant gas is allowed to flow through the system, down to the pressure regulator, and on into the primary portion of the test assembly. Concept 2 is similar to Concept 1 except that in this case the gas is admitted to the reservoir and then heated. See Appendix D for the governing equations and a sample calculation for this system. Concept 1 is the recommended design primarily because the convective heat transfer coefficient of the pebbles rises sharply with the increased flow velocity of system 1 as opposed to system 2 thereby allowing one to use fewer pebbles and to reduce the total amount of energy input to the reservoir.

REFERENCES

1. Shorr, M. and A. J. Zaehring, Solid Rocket Technology, Wiley (Chap. 7), "Thrust Vector Technology," by A. Brinsmade, 1967, pp. 209-236.
2. Sterrett, J. R. et al., "Experimental Investigation of Secondary Jets from Two-Dimensional Nozzles with Various Exit Mach Numbers for Hypersonic Control Applications," NASA TN-D-3795, January 1967.
3. Romeo, D. J., "Aerodynamic Interaction Effects Ahead of Rectangular Sonic Jets Exhausting Perpendicularly from a Flat Plate into a Mach Number 6 Free Stream," NASA TND-1800, May 1963.
4. Spaid, F. W., and E. Zukoski, "A Study of the Interaction of Gaseous Jets from Transverse Slots with Supersonic External Flows," AIAA J., Vol. 6, No. 2, February 1968.
5. Maurer, F., "Interference Effects Produced by Gaseous Side-Jets Issuing into a Supersonic Stream," TG 230-T460, 22 November 1965.
6. Werle, M. J., R. T. Driftmyer and D. G. Shaffer, "Jet-Interaction-Induced Separation of Supersonic Turbulent Boundary Layers - The Two-Dimensional Problem," AIAA Paper No. 70-765, Los Angeles, June-July 1970.
7. Goethert, B. H., and L. T. Barnes, "Some Studies of the Flow Pattern at the Base of Missiles with Rocket Exhaust Jets," AEDC-TR-58-12 (AD 302 082), Tullahoma, Tenn., October 1958.
8. Lott, R. A., et al., "Power-On Base Pressure for Space Shuttle Launch Configurations," LMSC-HREC D225152, Lockheed Missiles & Space Company, Huntsville, Ala., June 1971.
9. Baker, L. R., and W. H. Sims, "A Preliminary Plan for the Parametric Investigation of the Gasdynamic Effects on the Base Environment of Multi-Engine Vehicle Configurations," LMSC-HREC D225136, Lockheed Missiles & Space Company, Huntsville, Ala., June 1971.
10. Street, Troy A., "Status Statement of Reaction Jet Work Unit as of 1 January 1970," RD-TN-70-3, U.S. Army Missile Command, Redstone Arsenal, Ala., January 1970.
11. Schetz, Joseph A., and F. S. Billig, "Penetration of Gaseous Jets Injected into a Supersonic Stream," J. Spacecraft Roc., Vol. 3, November 1966, p. 1658.

12. Zukoski, E. E., and F. W. Spaid, "Secondary Injection of Gases into a Supersonic Flow," Guggenheim Jet Propulsion Center Report, California Institute of Technology, Pasadena, October 1963.
13. Cassel, L. A., et al., "Jet Interaction Control Effectiveness for Subsonic and Supersonic Flight," RD-TR-69-21, U. S. Army Missile Command, Redstone Arsenal, Ala., September 1969.
14. Thayer, W. J. III, "The Two-Dimensional Separated Flow Region Upstream of Inert and Chemically Reactive Transverse Jets," D1-82-1066, Boeing Scientific Research Laboratory, Seattle, March 1971.
15. Broadwell, J. E., "Analysis of the Fluid Mechanics of Secondary Injection for Thrust Vector Control," AIAA J., Vol. 1, No. 5, May 1963, pp. 1067-1075.
16. Wilson, W. G., and R. A. Comparin, "Analytical Investigation of Side Jet Supersonic Stream Interaction Including Vortex Flow in Rocket Nozzles for Thrust Vector Control," NASA CR 66754, June 1969.
17. Vaughan, J. C. III, "A Two-Dimensional Study of the Jet Interaction and Downstream External Burning Resulting from a Gaseous Sidejet Expanding into a Supersonic Airstream," TM-70-5, Jet Propulsion Center, Purdue University, West Lafayette, Ind., June 1970.
18. Korst, H. H., W. L. Chow and G. W. Zumwalt, "Research on Transonic Flow of a Real Fluid at Abrupt Increase in Cross Section," ME-TN-392-5, University of Illinois, Urbana, December 1959.
19. Dahm, T. J., "A Comprehensive Analytical Procedure for the Performance Prediction of Rocket Thrust Vector Control with Gaseous Secondary Injection," AFRPL TR-67-169, 1 June 1967.
20. Sakauri, A., "On the Propagation and Structure of a Blast Wave-I," J. Phys. Soc. Japan, Vol. 8, No. 5, September-October 1953.
21. Sakauri, A., "On the Propagation and Structure of a Blast Wave-II," J. Phys. Soc. Japan, Vol. 9, No. 2, March-April 1954.
22. Walker, R. E., and M. Shandor, "Influence of Injectant Properties for Fluid-Injection Thrust Vector Control," J. Spacecraft Roc., Vol. 1, No. 4, July-August 1964.
23. Dahm, T. J., "Data Analysis and Performance Prediction for the Thiokol Chemical Corporation TU-121 Motor Hot Gas Secondary Injection Thrust Vector Control Tests (U)," 9166-TN-6, Vidya Division of Itek Corp., Palo Alto, Calif., August 1964 (Confidential), AD 354 664.
24. Dahm, T. J., "The Development of an Analogy to Blast Wave Theory the Prediction of Interaction Forces Associated with Gaseous Secondary Injection into a Supersonic Stream," 9166-TN-3, Vidya Division of Itek Corp., Palo Alto, Calif., May 1964, AD 450 743.

25. Barnes, J. W. et al., "Control Effectiveness of Transverse Jets Interacting with High-Speed Freestream," Vol. 1, AFFDL TR 67-90, Wright-Patterson AFB, Ohio, September 1967.
26. Hair, L. M., and A. T. Baumgartner, "An Empirical Performance Model of Secondary Injection for Thrust Vector Control," LMSC-HREC A710184, Lockheed Missiles & Space Company, Huntsville, Ala., October 1964.
27. Whitacre, W. E., and R. W. Miller, "Secondary Injection Thrust Vector Control, Third Monthly Progress Report," LMSC-HEEC A033079, Lockheed Missiles & Space Company, Huntsville, Ala., October 1963.
28. Whitacre, W. E., and R. W. Miller, "Secondary Injection Thrust Vector Control - Fifth Monthly Progress Report," LMSC-HREC A033226, Lockheed Missiles & Space Company, Huntsville, Ala., December 1963.

Table 1
SITVC MATHEMATICAL MODELS

GAEC (Kaufman, 1968), 2-D
MDAC (Barnes, et al. 1967) 2-D
Martin (McDonald & Garbrick) 1966, 2-D
DVL (Maurer, 1965) 2-D Modified
U of M (Amick, et al. 1965), 2-D
GD (Dershin, 1965), 2-D
ARO (Strike, et al. 1963) 2-D, Circular
Lockheed (Hair & Baumgartner) 1964, 3-D
Aerotherm (Dahm, 1967), Circular
Vidya (Dahm, Mitchell, 1964), Circular
TRW (Broadwell, 1963) Circular
NASA (Sterrett, et al. 1966) 2-D
Lockheed (Carter & Culp, 1970), 3-D

Table 2

BASIC ASSUMPTIONS USED IN LMSC THREE-DIMENSIONAL JI MODEL*

1. The inviscid flow properties upstream of the separation points (pre-stream) are known a priori.
2. The pre-stream flow is two-dimensional or axisymmetric, including the case of local two-dimensionality with respect to a particular streamline (pseudo two-dimensional).
3. The nozzle wall frictional effects on plume properties are presently neglected.
4. The shear layer which characterizes flow separation is of the constant pressure type and is either pure laminar (Chapman) or fully developed turbulent (Korst). The shear layer developed along the plume boundary is considered to be the latter in view of the highly turbulent nature of most exhaust plumes.
5. The average flow velocity within the separation region is very low (dead-air) and the average pressure therein can be represented by the plateau pressure. Thus, the stream-side and plume-side shear layers are subject to the same external pressure (plateau pressure) under steady-state conditions.
6. The Prandtl, Schmidt, and Lewis numbers are unity, thereby rendering the generalized Crocco relation valid. The variation of species concentrations or relative mixture ratios across the shear layer can be determined in a similar manner. The inclusion of mixing effects in the 3-D program has not been completed.
7. The base temperature and the fuel-to-air ratio can be defined where the injector angle is such that the dividing streamlines of the separated flow shear layer and the plume boundary intersection produce weak oblique trailing shocks. Although afterburning is not likely to occur in the shear layer at high altitudes where long reaction and ignition delay times prevail, it is argued that equilibrium chemical reactions can be postulated in the dead-air region due to its low flow velocity and short characteristic ignition length.

* Lockheed, Carter & Culp, 1970.

Table 3

BASIC INPUT/OUTPUT TO LMSC THREE-DIMENSIONAL SLOT JET PROGRAM

BASIC INPUTLocal Mainstream

- Mach Number
- Static Pressure
- Static Temperature
- Gas Constant
- Ratio of Specific Heats

Exhaust Jet Properties

- Nozzle Exit Mach Number
- Stagnation Pressure
- Total Temperature
- Gas Constant
- Ratio of Specific Heats

Slot Geometry

- Length
- Width
- Injection Angle
- Area Ratio
- Nozzle Half Angle

BASIC OUTPUTJIM

- Upstream JI Force
- Upstream Amplification Factor
- Specific Impulse
- Downstream JI Force
- Jet Penetration Height
- Plume Induced Separation Distance
- Upstream Plateau and Peak Pressures
- Downstream Plate Pressure

JIM with Mixing (Current Development)

- TVC-Propellant Mixture Ratio in Upstream Separated
- Species Concentration
- Equilibrium Temperature

Table 4
SENSITIVITY TO INPUT PARAMETERS

a.*	Local Mainstream Mach Number, M_1	<ul style="list-style-type: none"> ● A_c increases with M_1 ● P_2/P_1 increases with M_1 ● A_c dependence decreases as M_1 increases ● I_{sp} increases with M_1 increasing
b.*	Local Mainstream Static Pressure, P_1	<ul style="list-style-type: none"> ● A_c increases with P_1 increasing ● A_c increases with P_{oj}/P_1 decreasing ● P_{oj}/P_1 decreases upstream separation distance ● P_{23}/P_2 decreases ● Jet penetrates proportionally higher
c.	Local Mainstream Static Temperature, T_1	<ul style="list-style-type: none"> ● Independent as long as γ_1 remains constant ● Significant with respect to external burning
d.	Local Mainstream Gas Constant, R_1	<ul style="list-style-type: none"> ● A_c independent of the mainstream gas constant ● Significant with respect to external burning
e.*	Local Mainstream Ratio of Specific Heats, γ_1	<ul style="list-style-type: none"> ● A_c increases with γ_1 ● A_c increases as γ_1 increases
f.	Jet Exit Mach Number, M_j	<ul style="list-style-type: none"> ● A_c varies only 1% as M_j goes from 1 to 2.5 ● At $M_j = 4P_\infty < P_1$ JI theory violated ● F_j increases and F_i decreases

*Most sensitive parameters for two-dimensional Jet Interaction (JI).

Table 4 - (Continued)

g.*	<p>Jet Stagnation Pressure, P_{Oj}</p> <ul style="list-style-type: none"> ● A_c increases as P_{Oj} decreases ● Smaller penetration \rightarrow reduces separation distance
h.	<p>Jet Total Temperature, T_{Oj}</p> <ul style="list-style-type: none"> ● A_c is independent of T_{Oj} same as T_1 ($\gamma = \text{const.}$) ● I_{sp} increases as the $\sqrt{T_{Oj}}$
i.	<p>Jet Gas Constant, R_j</p> <ul style="list-style-type: none"> ● A_c is independent of R_j same as R_1 ● I_{sp} increases as the $\sqrt{R_j}$ (and $\sqrt{T_j}$)
j.*	<p>Ratio of Specific Heats for the Jet, γ_j</p> <ul style="list-style-type: none"> ● A_c decreases as γ_j increases ● A_c decreased when γ_j increased <p> $V_t = a_j \sqrt{2/\gamma+1} = \sqrt{2\gamma/\gamma+1RT_{Oj}} \Rightarrow V_t$ decreases as γ_j increases $\dot{m} = \rho_t A_t V_t \Rightarrow \dot{m}$ decreases as γ_j increases $F = I_{spO} \dot{m} \Rightarrow F$ decreases as γ_j increases $F = -\dot{m} V_j + A_j (P_j - P_{Oj})$ C_F decreases with increase in γ_j, $F = P_{Oj} A_t C_F$ </p>
k.*	<p>Slot Throat Width, d_t</p> <ul style="list-style-type: none"> ● A_c increases with a decrease in d_t ● A_c decreases 7% with a 100% increase in d_t ● A_c decreases 5% with a 100% increase in P_{Oj} ● Increased d_t and P_{Oj} increases penetration
l.*	<p>Jet Injection Angle, $\alpha_j - 15$ to 30°</p> <ul style="list-style-type: none"> ● A_c increases as the jet is transversed to slightly upstream ● A_c decreased as the jet is transversed to slightly downstream ● θ_d decreases as α_j increases forward

*Most sensitive parameters for two-dimensional Jet Interaction (JI).

Table 5
 TYPICAL BOOSTER CONTOURED NOZZLE COORDINATES
 Propellant, LOX/RP-1; $P_c = 17.237 \times 10^5 \text{ N/m}^2$; (250 psia); O/F = 2.8

Local Nozzle Radius, R (meters)	Distance Along Nozzle Axis, X (meters)
0.8636*	0.0000
0.8819**	0.1110
0.8906	0.1367
0.9034	0.1737
0.9163	0.2105
0.9294	0.2471
0.9426	0.2837
0.9560	0.3203
0.9697	0.3572
0.9838	0.3943
0.9982	0.4318
1.0125	0.4697
1.0270	0.5081
1.0418	0.5472
1.0569	0.5871
1.0723	0.6280
1.0882	0.6698
1.1046	0.7130
1.1222	0.7577
1.1393	0.8035
1.1570	0.8510
1.1752	0.9002
1.1940	0.9514
1.2134	1.0047
1.2338	1.0605
1.2554	1.1192
1.2769	1.1802
1.2990	1.2441
1.3220	1.3114
1.3457	1.3822
1.3717	1.4577
1.3974	1.5367
1.4237	1.6202
1.4510	1.7087
1.4800	1.8033
1.5101	1.9041
1.5403	2.0111
1.5715	2.1258
1.6057	2.2510
1.7114	2.6874
1.7537	2.8868
1.8368	3.3148
1.8855	3.5977
1.9222***	3.8420
1.9430	3.9877

* Throat point; ** tangent point; *** exit point.

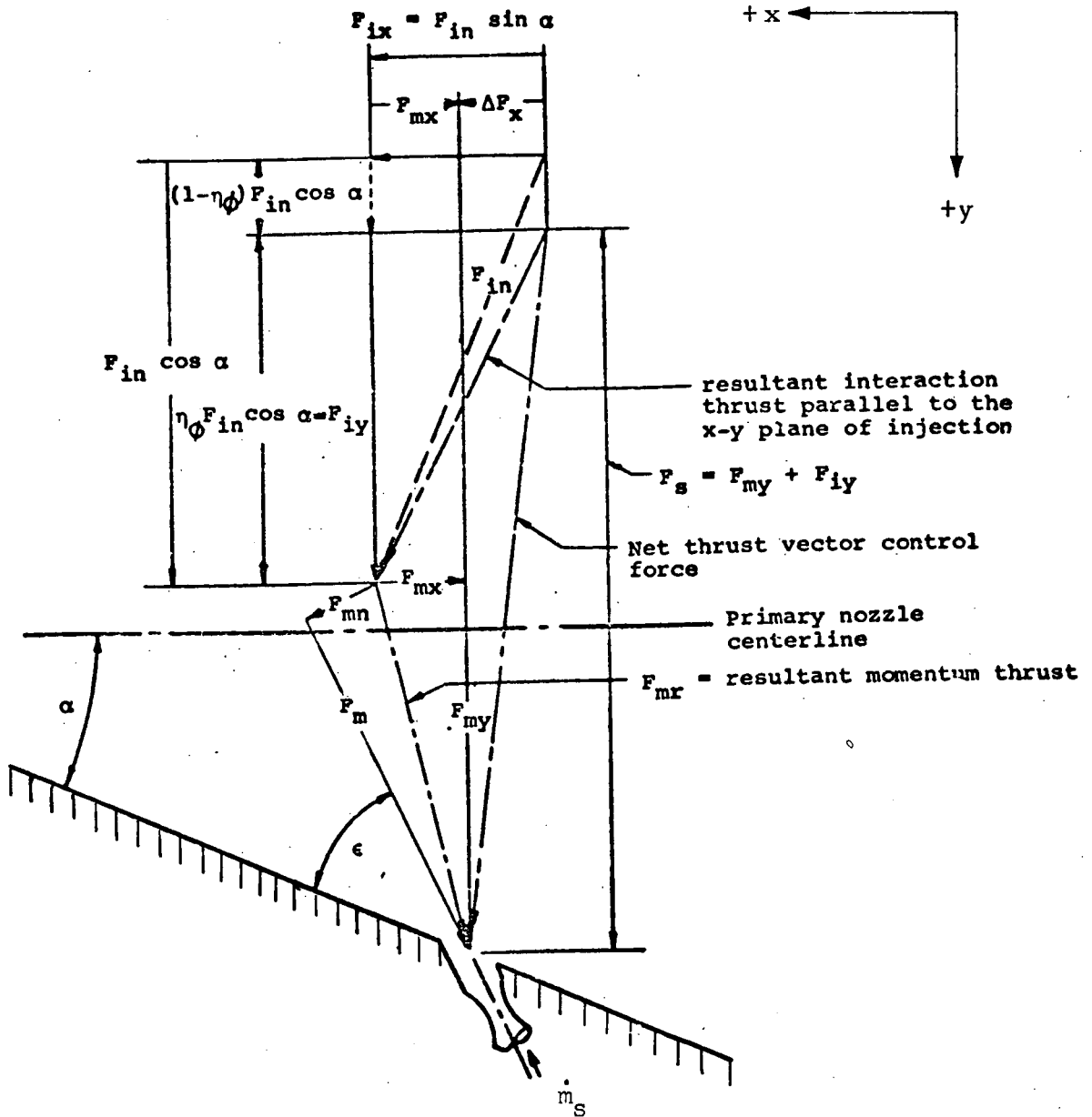


Fig. 1 - Component Diagram for Secondary Injection Thrust Vector Control Forces (Ref. 19)

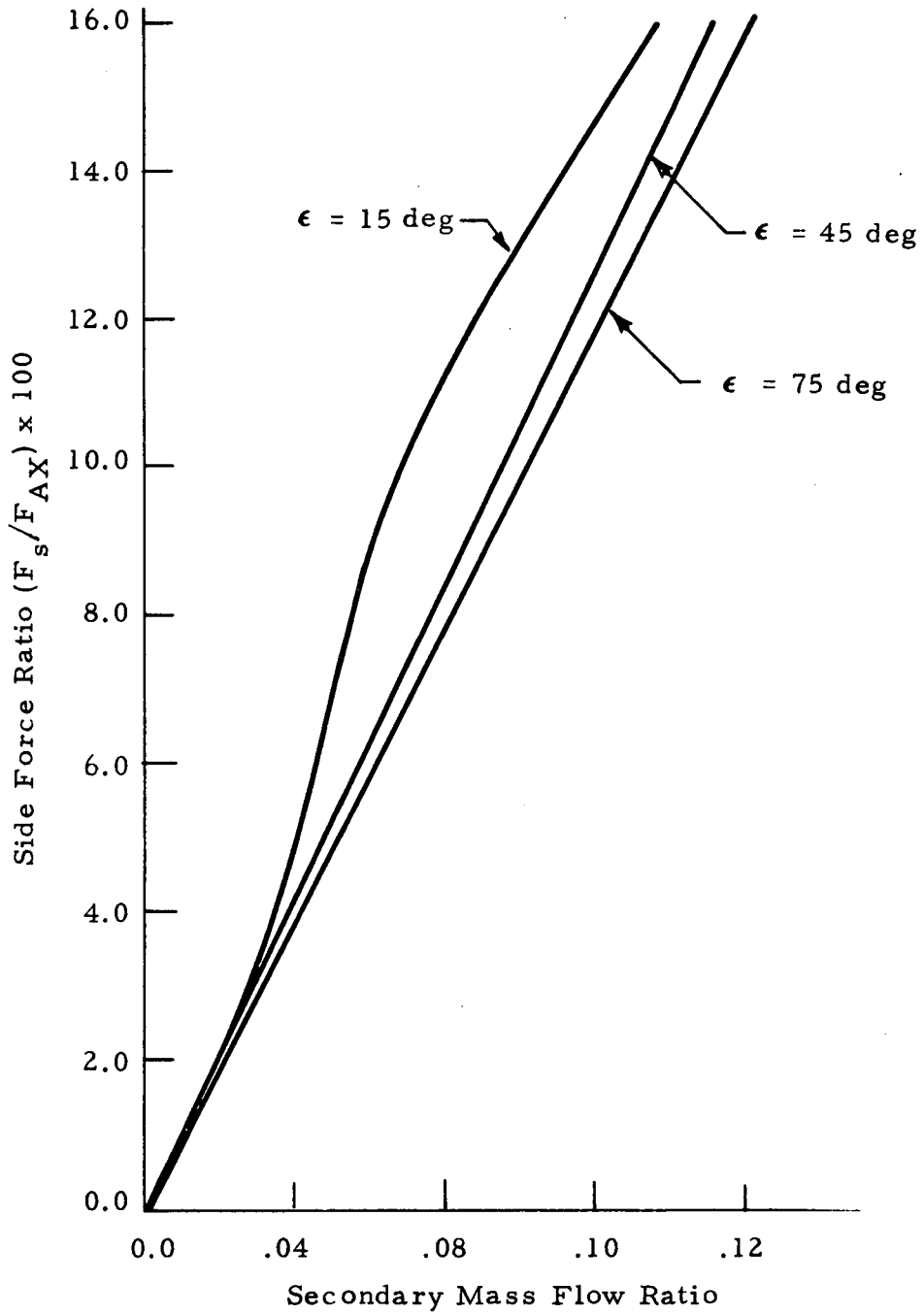


Fig. 2 - TVC Side Force Ratio vs Secondary Mass Flow Ratio
($X/L = 0.25$)

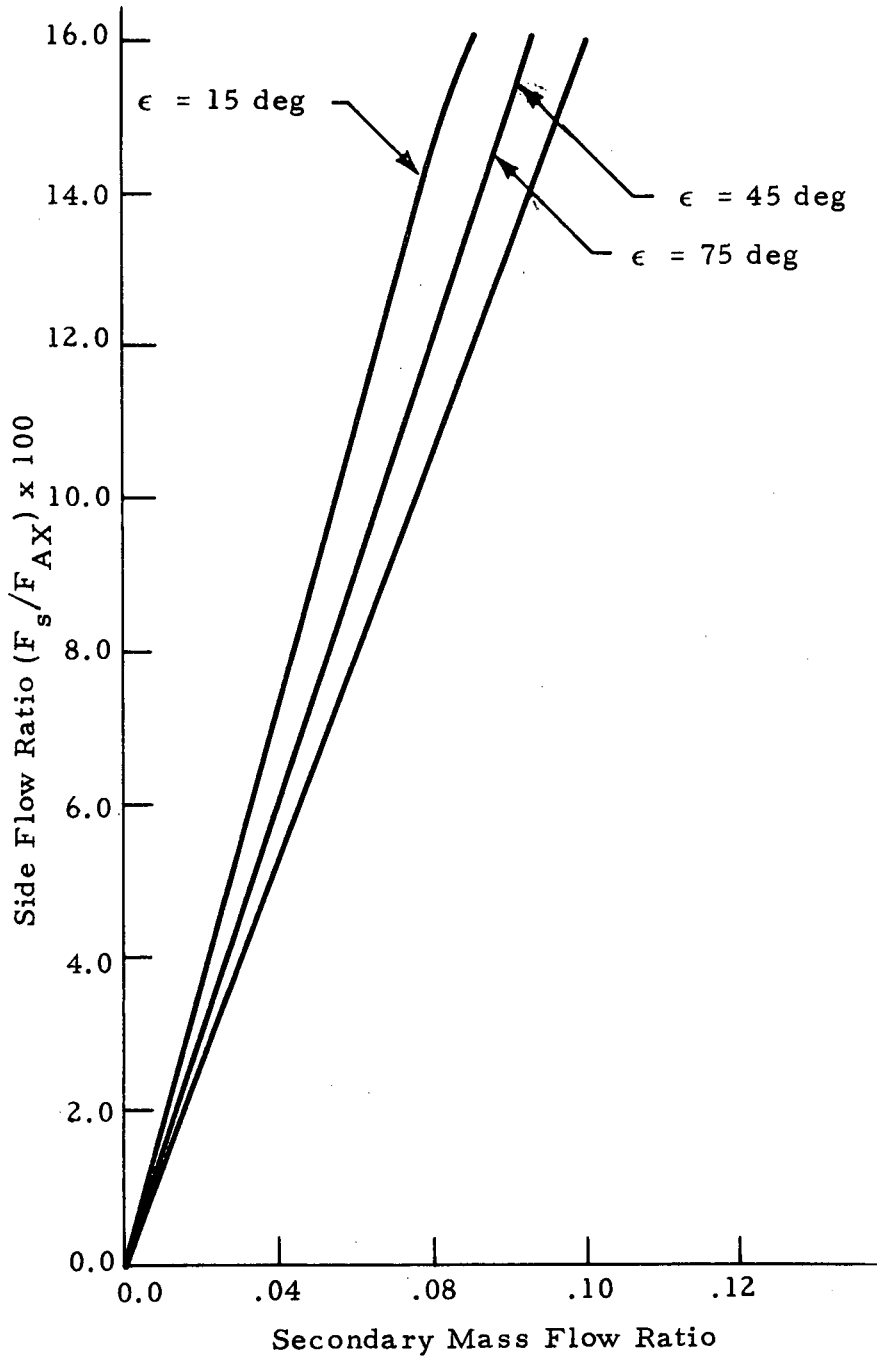


Fig. 3 - TVC Side Force Ratio vs Secondary Mass Flow Ratio (X/L = 0.50)

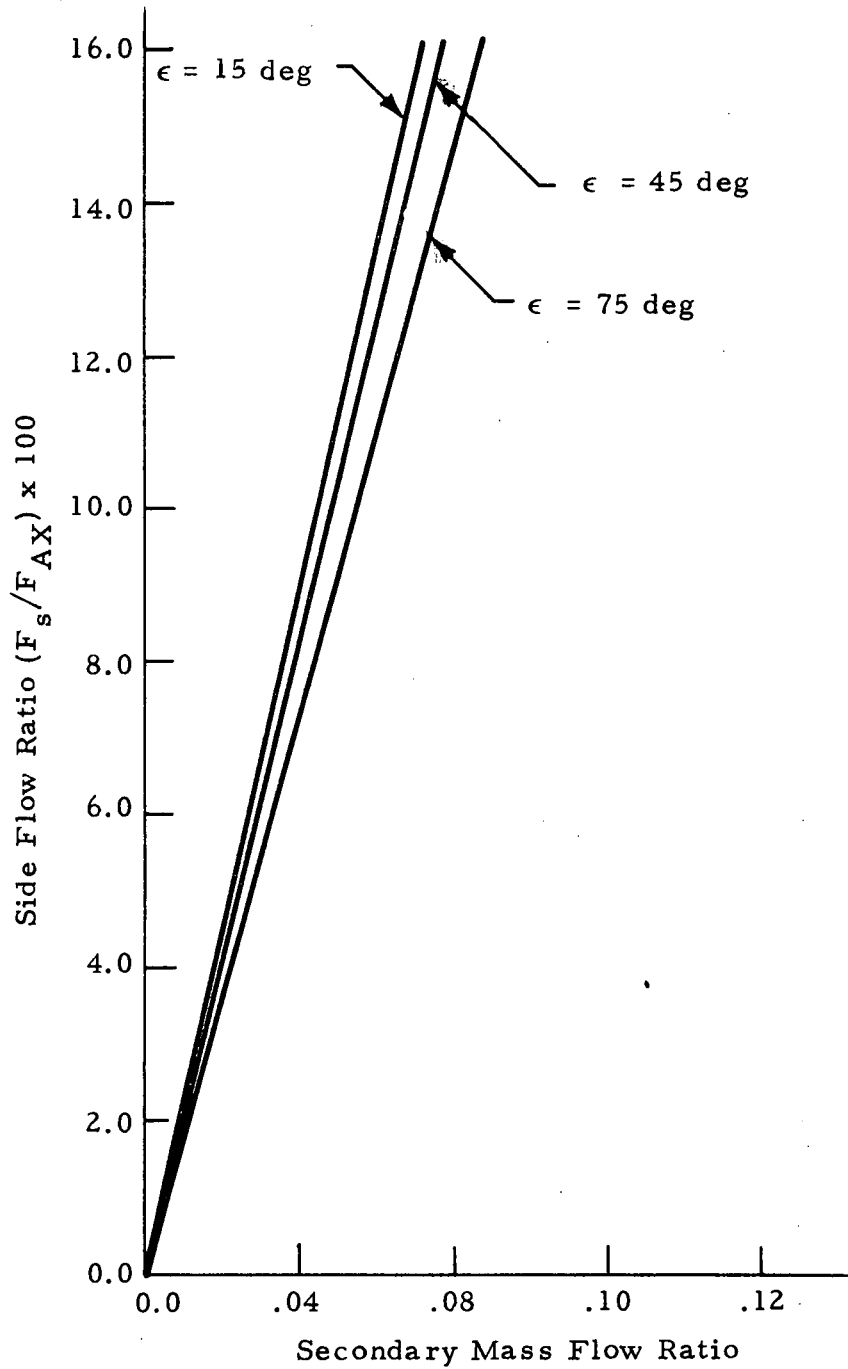


Fig. 4 - TVC Side Force Ratio vs Secondary Mass Flow Ratio
($X/L = 0.75$)

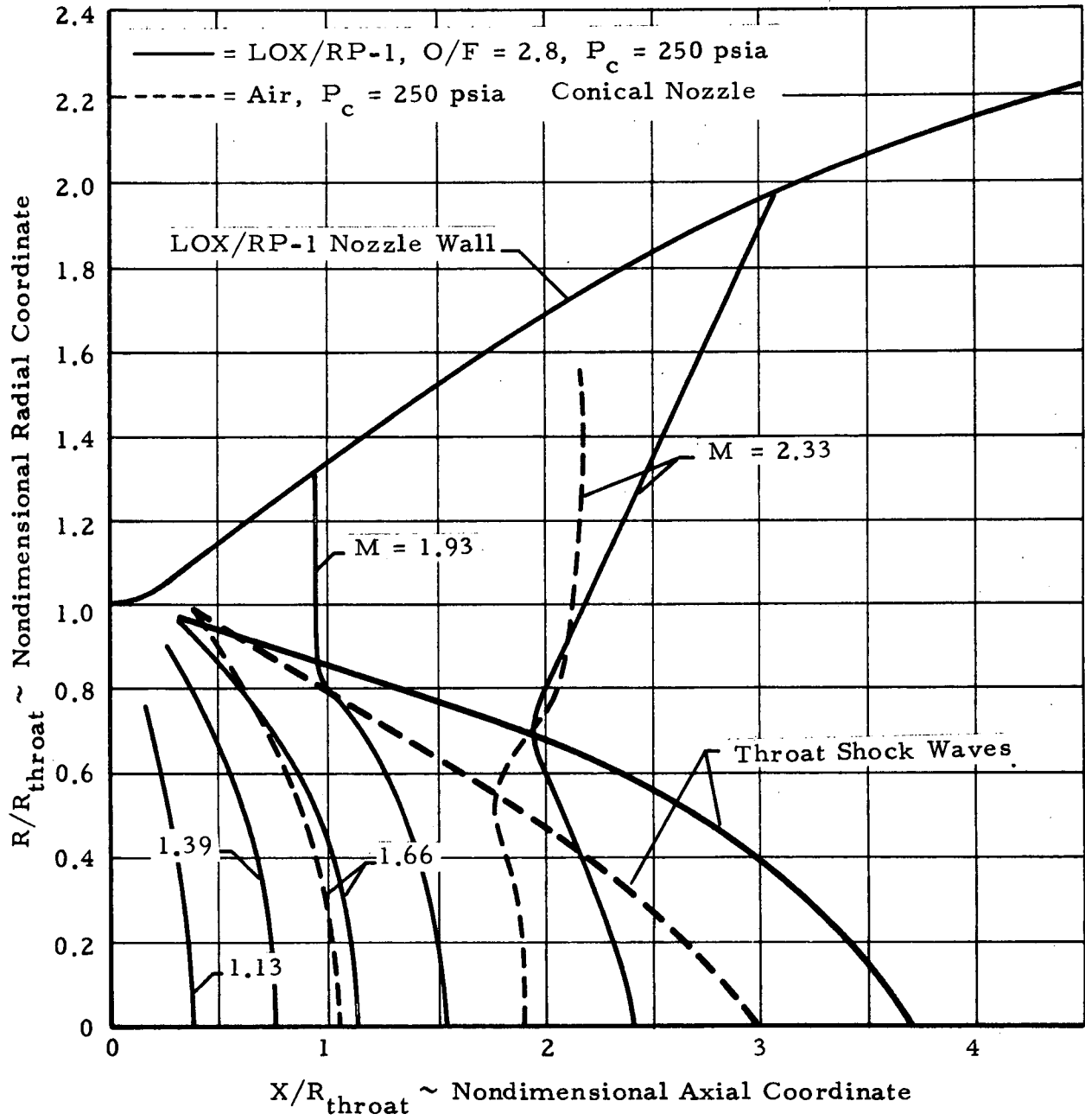


Fig. 5 - TVC Nozzle Constant Mach Number Contours

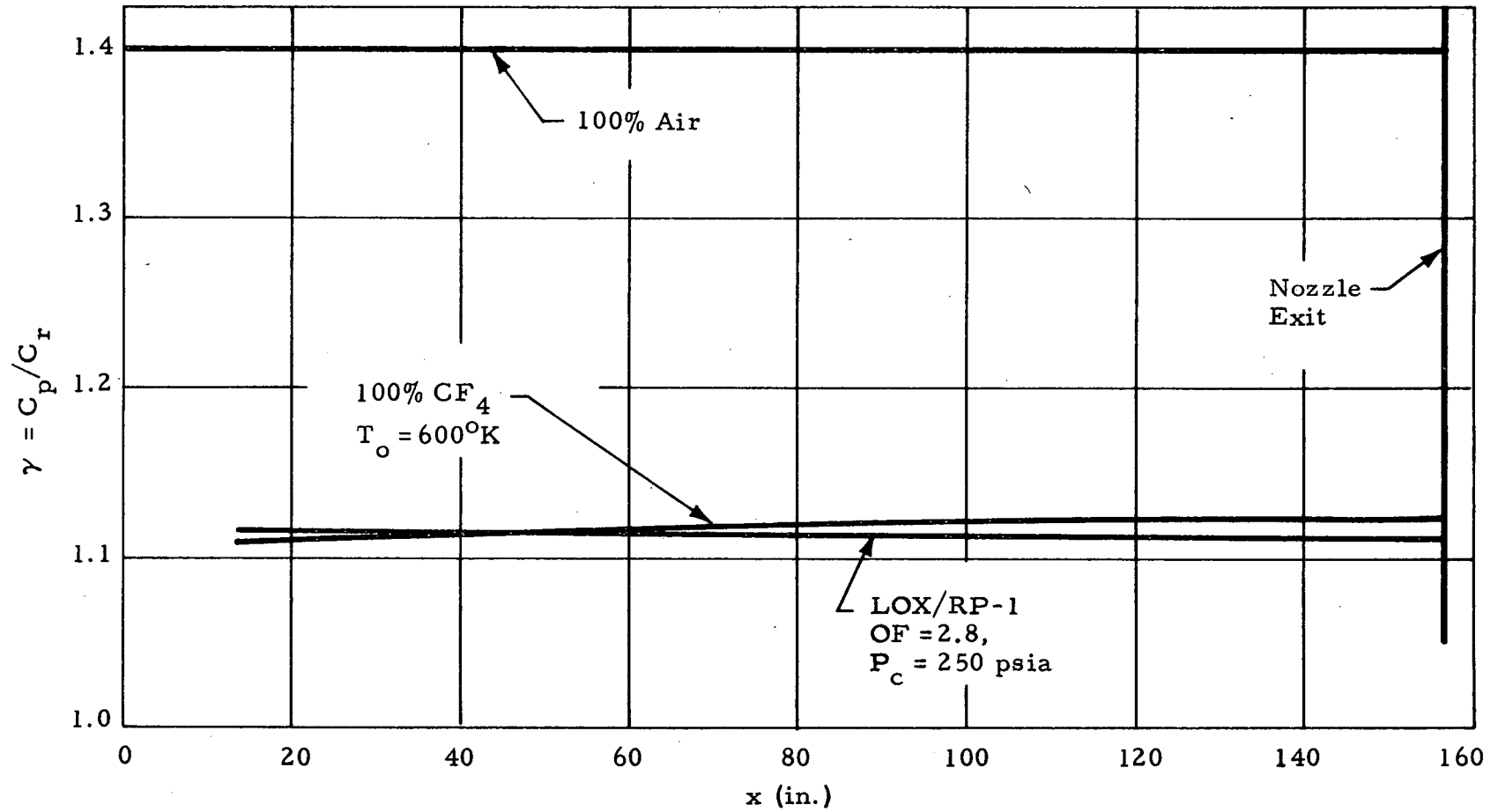
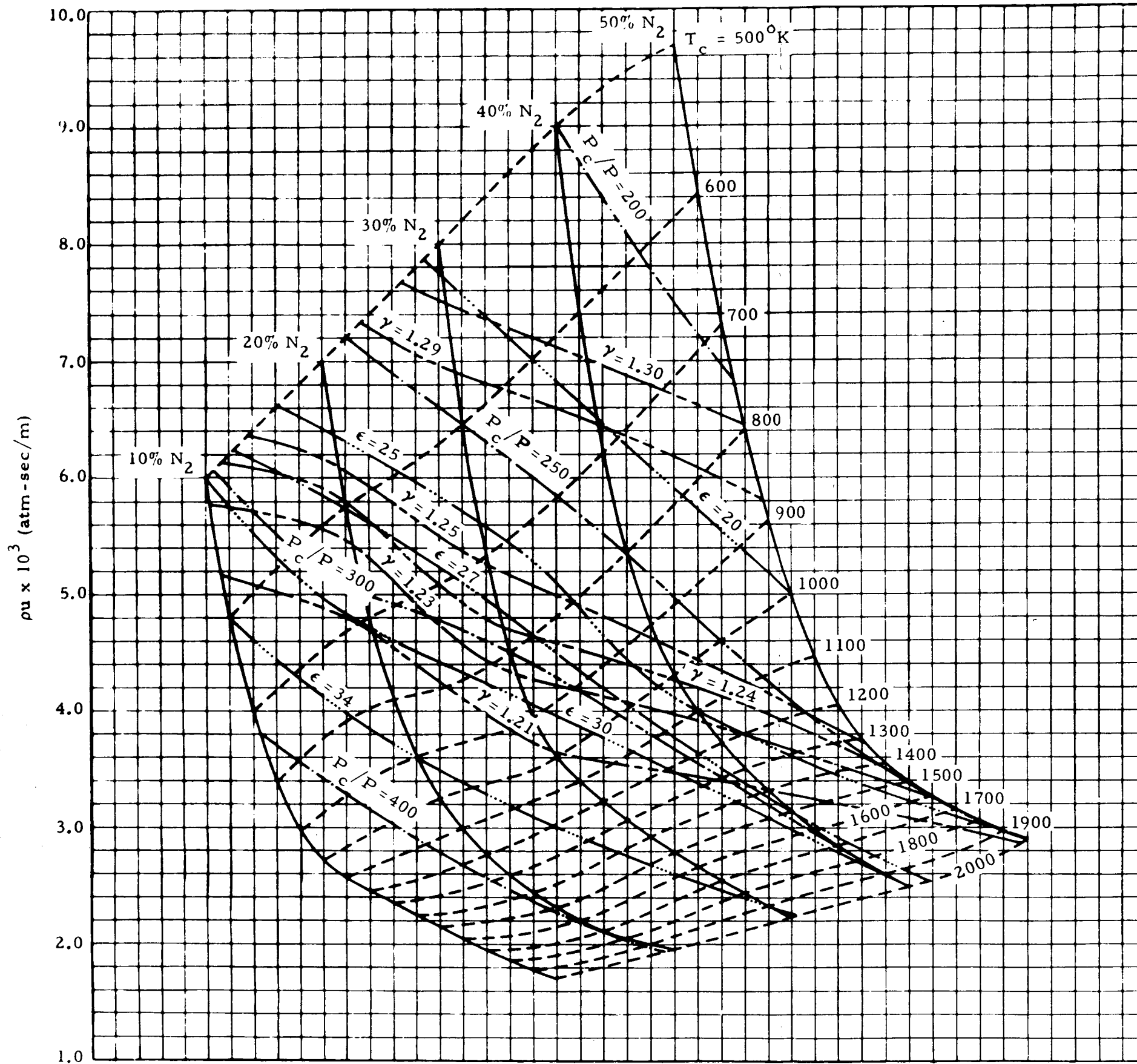


Fig. 6 - Variation of the Ratio of Specific Heats for a Typical Booster Engine



NOTE: Data shown were generated for a chamber pressure (P_c) of 1000.0 psia. To use for P_c conditions other than the above the values of " ρu " must be multiplied by ratio of $P_c/1000.0$.

Fig. 7 - Variation of the " ρu " Product at the Nozzle Exit Plane as a Function of Percent N_2 in Mixture of CF_4/N_2 and Chamber Temperature T_c ($M_{primary} = 3.9$)

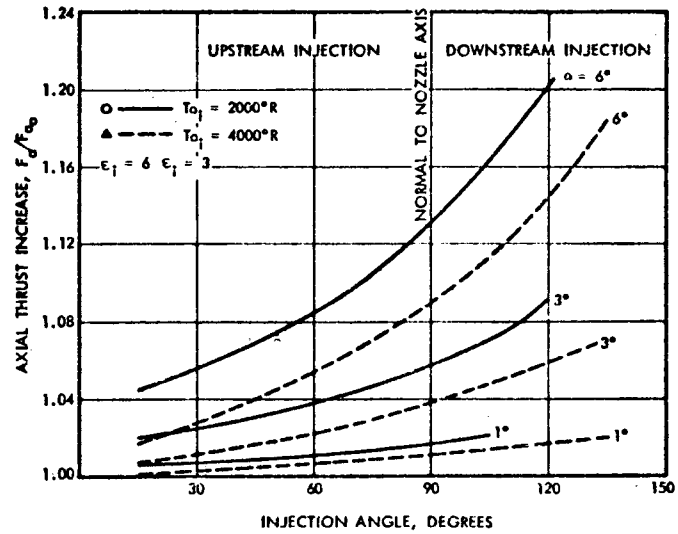
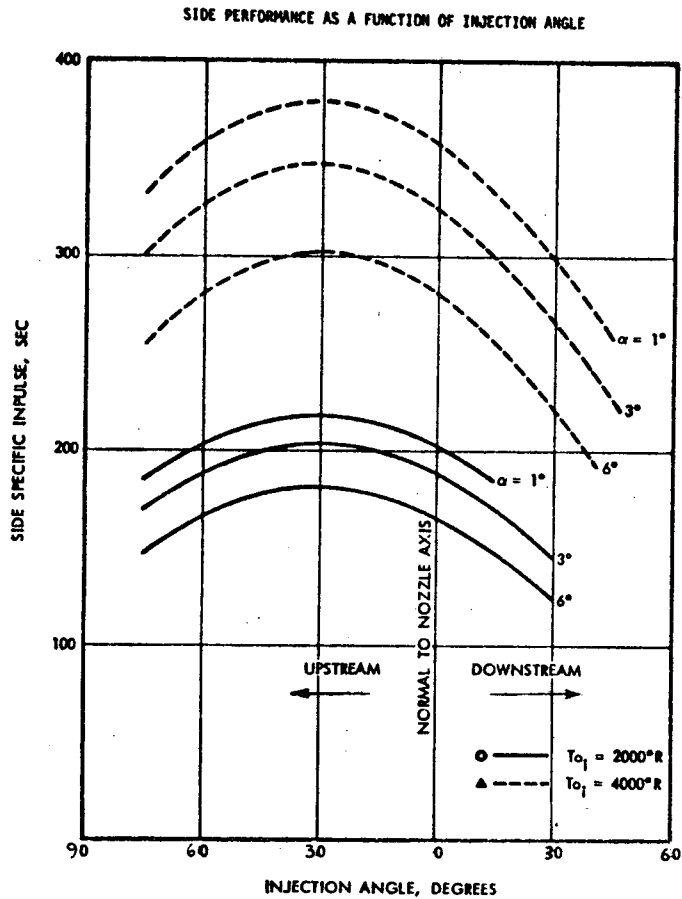
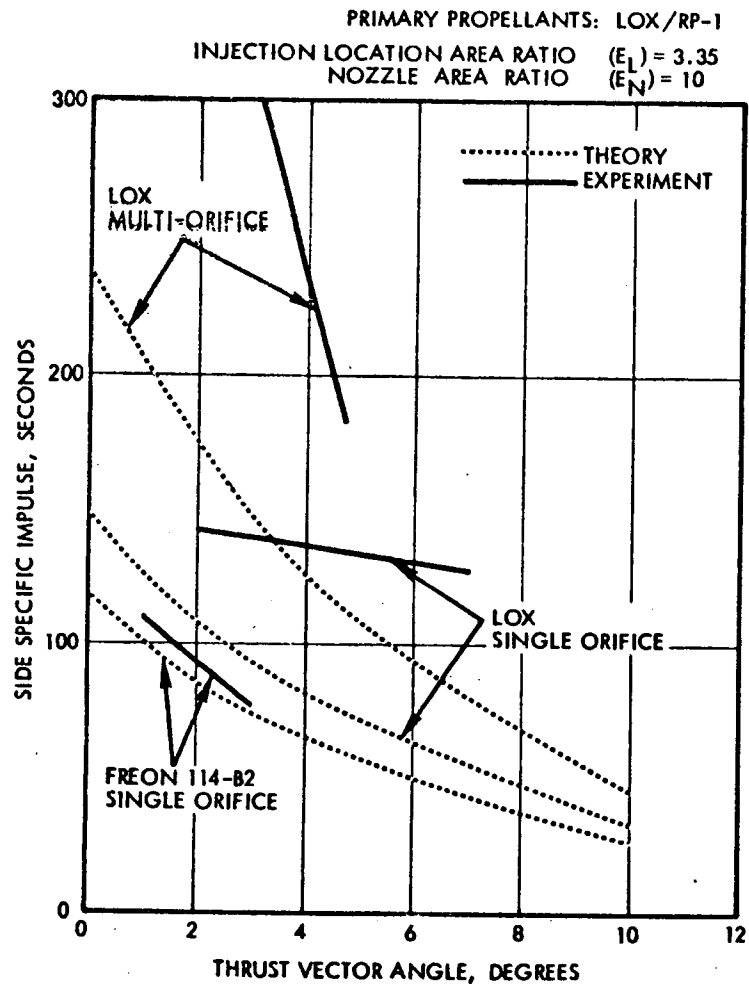


Fig. 8 - Effect of Injection Angle on TVC System Performance (Refs. 20 and 21)

SIDE SPECIFIC IMPULSE
VS
THRUST VECTOR ANGLE

THEORETICAL/EXPERIMENTAL DATA COMPARISON



EFFECT OF NUMBER OF ORIFICES ON SIDE SPECIFIC IMPULSE
DATA FROM CHAPMAN AND GRUNDWALD

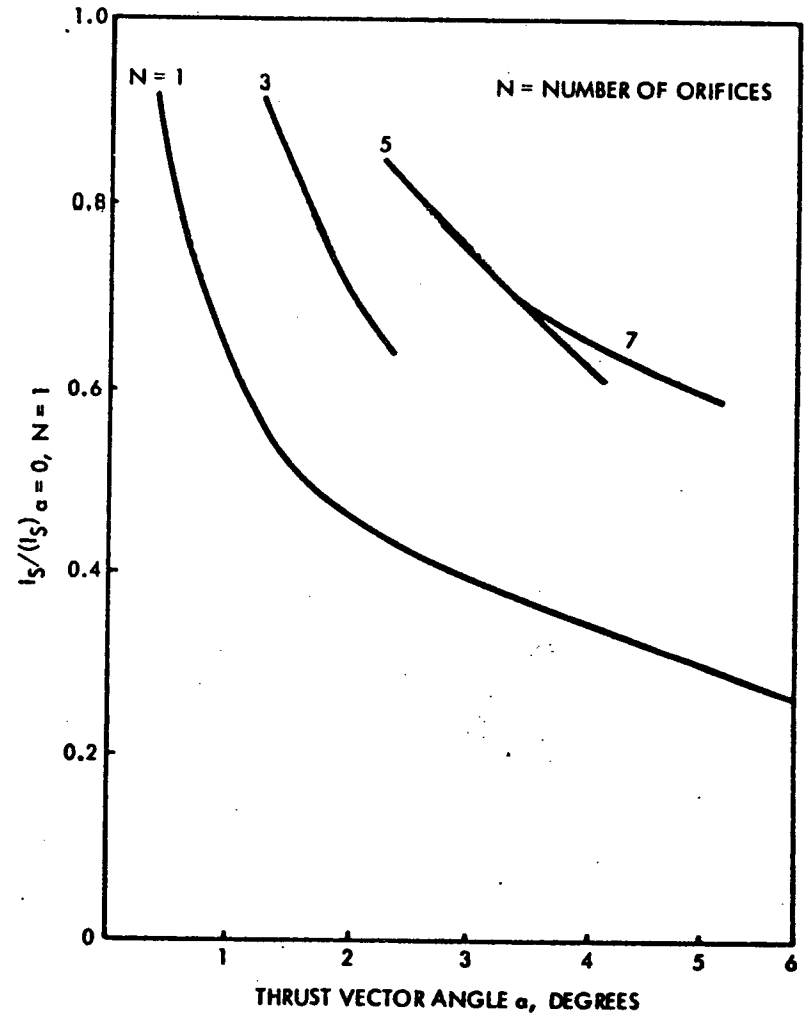


Fig. 9 - Effect of Multiple Orifices on TVC System Performance

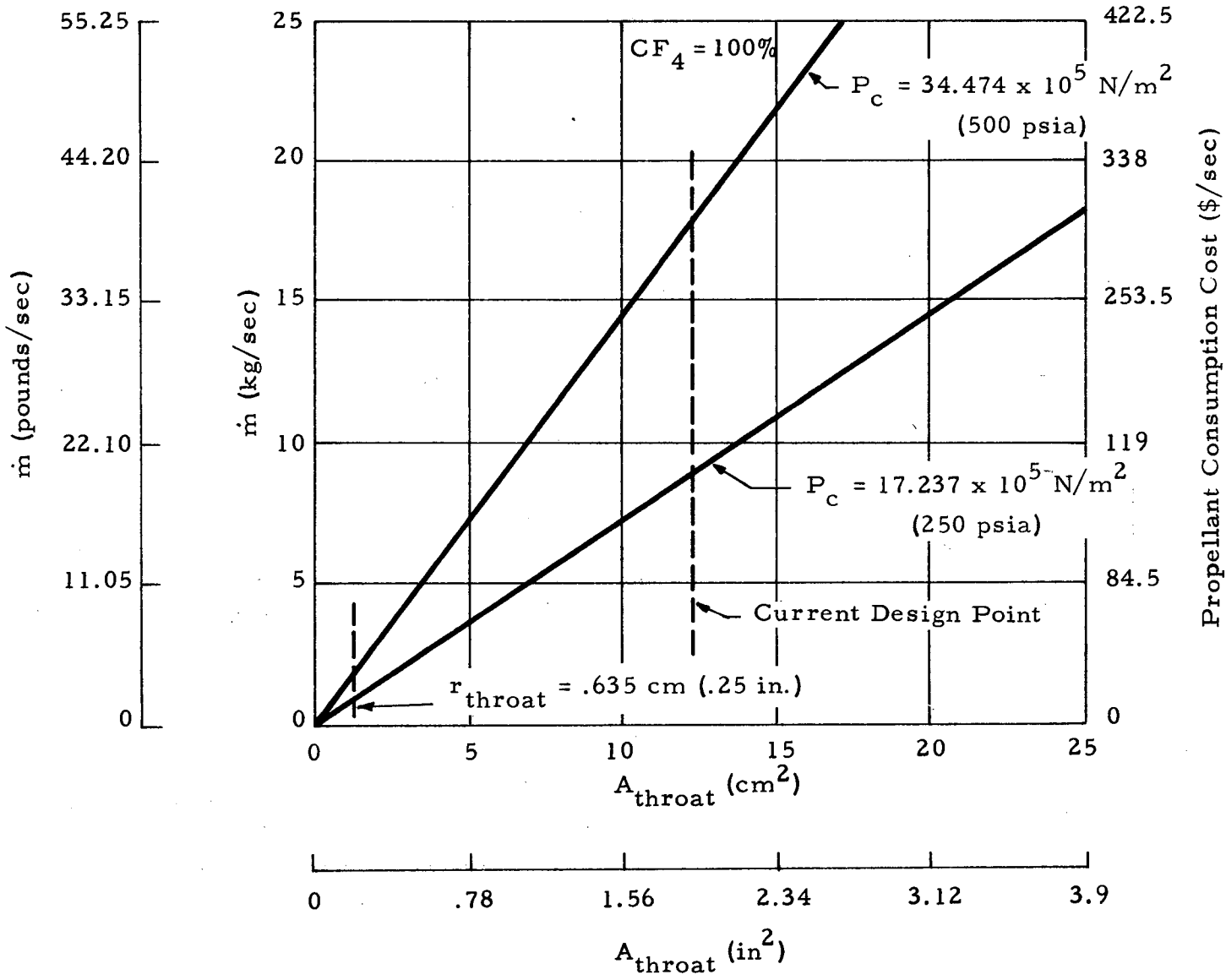


Fig. 10- Effect of Model Size on Test Facility Flow Rate and Operating Cost

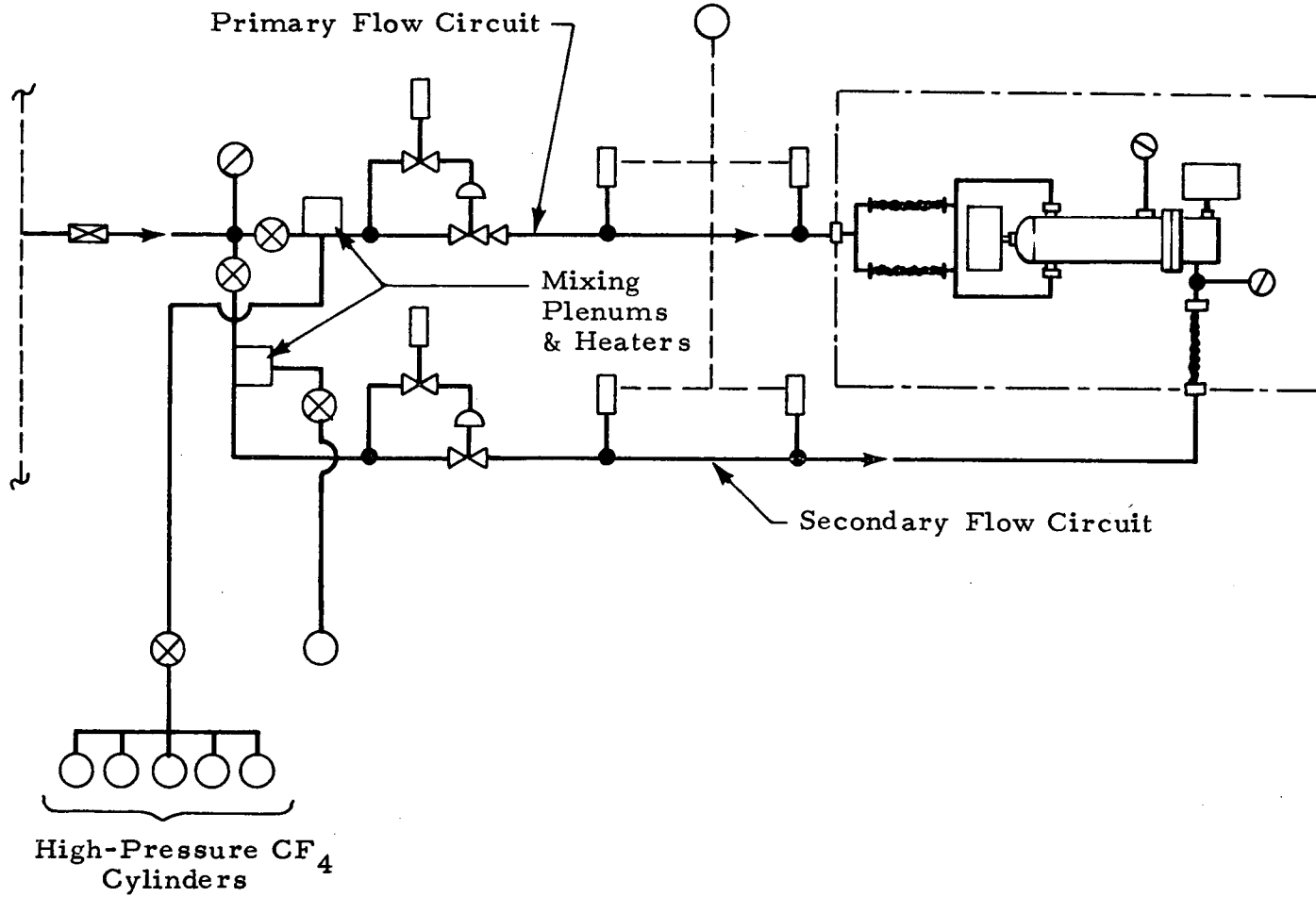


Fig. 11- Schematic of Thrust Vector Control Facility

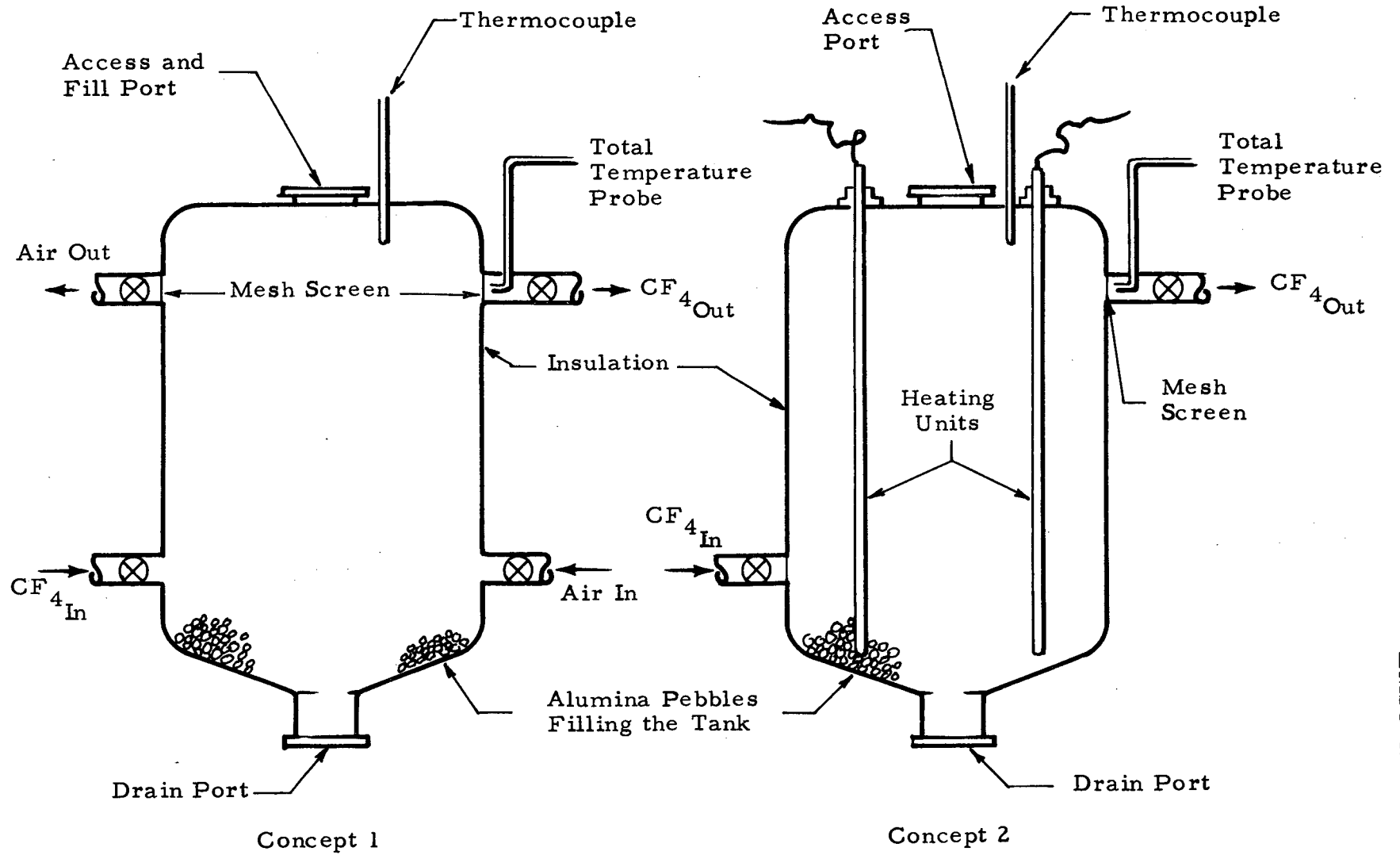


Fig. 12 - TVC Test Facility Heater

Appendix A

MODELING THE THREE-DIMENSIONAL EFFECTS
OF A SLOT JET FLOW FIELD*

* Lockheed internal research, prepared by R. E. Carter
and M. F. Culp, Sunnyvale, Calif., 1970.

CONTENTS

	Page
Introduction	1
Symbols and Nomenclature	2
Jet-Freestream Interaction Flow Field	5
Slot Span Flow	7
Baseline Two-Dimensional Model	7
Jet Penetration Height	9
Three-Dimensional Flow Field Model	12
Surface Curvature Approximation	18
Comparison to Maurer's Test Data	20
Comparison to Romeo's Test Data	22
Jet Interaction Computer Studies	24
Conclusions	30
Recommendations	31
References	32

ILLUSTRATIONS

Figure		Page
1	Jet Freestream Interaction	6
2	View Looking Down on Jet Transverse to Flow	8
3	Boundary Layer Separation Distance vs. Pressure Ratio . . .	11
4	Control Volume	13
5	Maurer, Mach Equal 1.57 Comparisons	21

ILLUSTRATIONS (Continued)

Figure		Page
6	Romeo, Mach Equal 6 Comparisons	23
7	Aspect Ratio 10, Mach Equal 5 Parametric	27
8	Aspect Ratio 10, Mach Equal 5 Parametric	27
9	Aspect Ratio 10, Mach Equal 5 Parametric	28
10	Aspect Ratio 10, Mach Equal 5 Parametric	28
11	P_{oj}/P_1 Equal 80	29

INTRODUCTION

Preliminary engineering estimates and experiments on flat plates have amply demonstrated that the injection of a jet of fluid, either reacting or non-reacting, transverse to the free stream flow over a surface can produce forces greater than the jet thrust alone. Such forces are achieved by separating the boundary layer ahead of the jet. The use of non-reacting transverse jets for force generation has commonly been termed jet interaction. Numerous jet interaction tests have been conducted with application to supersonic vehicle reaction control systems and thrust vector control of rocket motors. Similar jet interaction phenomena exists when a jet is fired forward for thrust termination, when gases escape from a missile stage, and when a highly expanded rocket motor plume induces boundary layer separation.

Jet interaction forces have been mathematically modeled by many investigators but their methods are limited to two-dimensional or modified two-dimensional slot flow situations. Relatively little attention has been given to the behaviour and structure of a three-dimensional model. Unfortunately, the application of a two-dimensional model to a three-dimensional reaction control system cannot be made without first determining, by testing techniques, several empirical correlation factors. It is therefore believed, by the authors of this article, that a basic understanding of the three-dimensional effects of the jet interaction phenomenon is required before significant improvements to the state-of-the-art technology can be made. This analysis provides a three-dimensional model that can be easily expanded to include other jet interaction effects such as external burning, viscous mixing, and downstream effects.

SYMBOLS AND NOMENCLATURE

A^*	sonic area
A_e	cross-section area for end flow model
A_g	geometric area at slot span, figure 4
A_∞	area where slot span flow reaches freestream conditions
a_j^*	jet gas velocity ($M = 1$)
AR	aspect ratio or b/dt
b	slot half span, figure 2
b/dt	aspect ratio - slot half span to width ratio
BA	width of modified two-dimensional region II, figure 2
C_{f_0}	thrust coefficient of jet nozzle
Cn	Maurer amplification factor
$C_{N,A}$	normal force ahead of slot jet
$C_{N,R}$	normal force of jet alone
dA	surface area over which end flow acts
dt	width of nozzle throat, figure 2, 3
dy	increment of span - unit length, figure 4
dQ_s	slot span flow
FU	interaction force in front of the slot
FUE	interaction force at the slot end
FJ	jet reaction thrust of slot
FJO	vacuum jet reaction thrust of slot
FN	incremental strip force

h , or $h_{(y)}$	jet penetration height
h_s	new jet penetration height with slot span flow
h_o	penetration height at slot centerline (ellipse semi-minor axis)
h_b	penetration height at slot span end
i	number of selected strips
J	constant equal to 0.88, reference 6
JIB	jet interaction with burning
K	amplification factor, $\frac{FJ \cos \phi + FU}{FJO}$, no end effects
K_T	amplification factor with end effects
L	reference length, distance from leading edge of plate to slot
M_∞	freestream Mach number, figure 1
M_1	local freestream Mach number, figure 1
M_2	Mach number of inviscid flow above separation region, figure 1
M_e	nozzle exit Mach number, figure 3
\dot{m}_i	slot span mass flow rate
\dot{m}_o	slot span mass flow at freestream conditions
N	$dy - 1$, number of strips = 10
P_1	local pressure before separation
P_2/P_1	plateau pressure ratio
P_3	pressure behind the jet
P_4	downstream pressure behind the jet
P_{oj}	jet plenum total pressure
P_R	reattachment pressure ratio
$q_1 = \frac{\gamma}{2} P_1 M_1^2$	local freestream dynamic pressure
R'	body radius of slot (cone or cylinder)
R_e	radius as defined in equation 11, figure 2
R_n	Reynolds number (laminar $< 1 \times 10^6$, turbulent $> 5 \times 10^6$)

S	as defined in equation 7
T_1	Local freestream temperature, °R
V_1	local freestream velocity
V_2	velocity over the penetrating jet
V_e	nozzle velocity at exit to throat sonic velocity
x, y, z	slot coordinate system, figure 4
X_s	separation distance, figure 2
X	new separation distance with slot span flow
X_e	x-axis for blast wave radius, figure 2
α	empirical parameter (suggested 1.2)
δ	cone half angle
σ	separation ramp angle
σ_b	separation flow angle at slot span end
β	$\beta' \gamma M_2^2 / (1 + \frac{\gamma - 1}{2} M_2^2)$
β'	empirical parameter (suggested 0.062)
ϕ	inclination of nozzle centerline relative to an axis normal to the surface, figure 4
θ	body angle in z, y plane, $\frac{y_{N-1} + \frac{1}{2} (y_N - y_{N-1})}{R'}$ 57.3
γ, γ_j	ratio of specific heats, freestream or jet
ϵ	cross flow parameter
ϵ_o	cross flow parameter at slot centerline
ϵ_b	cross flow parameter at end of slot
2-d	two-dimensional flow, figure 2
ρ_1	local density before separation
ρ_2	density over the penetration jet

Jet-Freestream Interaction Flow Field

The phenomenon of a supersonic jet injected into a supersonic freestream has been described by many investigators, references 1-9. Figure 1 schematically defines, in a profile view, the major features of this jet interaction flow region. The five major areas of interest in this figure are:

- The plume-induced separated flow in the upstream circulatory region (6) that increases the reaction force greater than the vacuum thrust of the injectant.
- The inviscid jet plume flow that is two-dimensional in the case of a slotted entrance duct (9), or axisymmetric, in the case of a square port.
- The penetration mixing region that results from viscous mixing between the freestream and the region above the jet normal shock wave (12).
- The downstream base circulatory region (11) that also effects the force amplification of the reaction control system.
- The downstream recompression region (19) that is dependent upon the over-expanded gas (16) in the penetration mixing region.

Slot Span Flow

If the jet-freestream interaction is two-dimensional, there will be no flow around the end of the jet exit. When flow does occur around the slot ends, the term "slot span flow" is used, and a slot aspect ratio effect upon jet interaction performance is apparent. Figure 2 schematically illustrates the elliptical line of flow separation and four major regions of interest:

- The two-dimensional region (I), with no slot span flow, can exist near the centerline of the slot for high aspect ratio slots with sufficiently low jet penetration. However, in some cases this region may not exist at all.
- The modified two-dimensional region (II), with increasing slot span flow, can exist for low aspect ratio slots and sufficiently high jet penetration.
- The slot span flow is expanded around the end of the slot in region (III) until the sonic slot span flow reaches freestream conditions.
- The downstream region (IV) that realizes viscous mixing between the end flow and the downstream region of figure 1.

Baseline Two-Dimensional Model

A jet interaction literature search revealed that the two-dimensional analytical method developed by Barnes¹ was the best presently available. This mathematical program was therefore selected as baseline for improvement since its format could be easily modified to account for three-dimensional effects. This mathematical model has the ability to calculate the additional force produced by boundary layer separation that results from a gas jet injected through an infinitely long slot in a flat plate surface into a uniform supersonic stream.

LEGEND

- I** 2-d REGION - MDAC AND OTHERS
- II** MODIFIED 2-d REGION
- III** END EFFECT
- IV** DOWNSTREAM REGION-HIGHLY EMPIRICAL

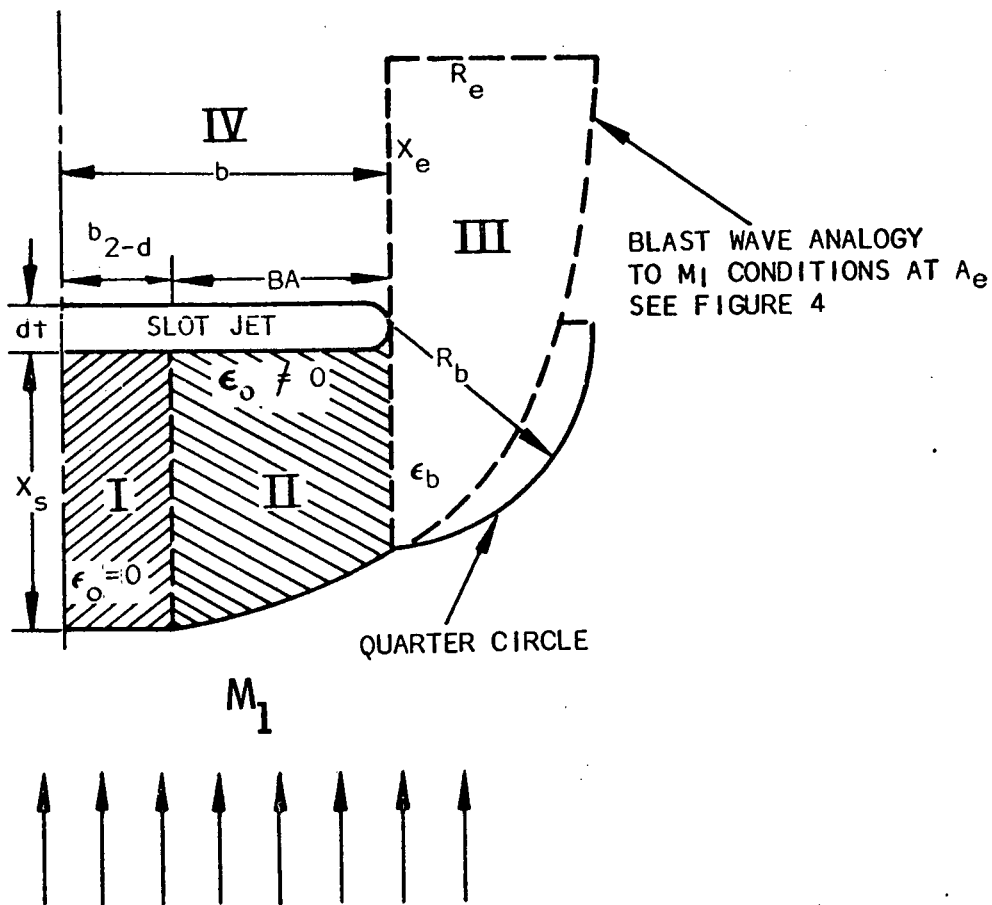


Figure 2 View Looking Down on Jet Transverse to Flow

The baseline model uses a two-dimensional momentum balance between a transverse slot jet and the surrounding supersonic freestream. The momentum balance consists of equating the drag on the equivalent body formed by the transverse jet interaction to the change in axial momentum of the transverse jet. This model assumes that the viscous portion of the drag is proportional to the reattachment pressure coefficient while the inviscid contribution (deflection of the freestream) is proportional to the plateau pressure coefficient. The total drag coefficient is related to these parameters by empirical constants. The model computes the jet penetration height (h_o) of the injected gas, the point of freestream flow separation (X_s) in front of a flat plate slot with end plates, and the force amplification (K). These parameters are a function of the plume-induced separated flow for local laminar or turbulent freestream Reynolds numbers, jet and freestream gas properties, and freestream Mach number.

Jet Penetration Height

The first modification to the two-dimensional baseline model involved a new method² of calculating the penetration height (h) of a transverse jet. To do this, the plateau pressure (P_2) can be computed using the curve fit of Barnes¹ for pressure coefficient. Both the laminar and turbulent flow values have been mechanized and can be computed as a function of Mach number. The plateau pressure is modified by a new constant (β) which is representative of the reattachment pressure on a forward facing step. The pressures on the back side of the jet are analogous to the base pressure of a step and the constant (α) is used to represent the base pressure to freestream pressure ratio. The sum of the forward and backward face pressures is then the total force acting on the jet in the streamwise direction.

The penetration height (h) calculation is therefore no longer dependent on the baseline equivalent body drag coefficients and empirical constants of Barnes¹:

$$h = dt \frac{\gamma \left(\frac{2}{\gamma+1} \right)^{\frac{\gamma-1}{2}} \left(\frac{P_{oj}}{P_1} \right) \left(1 + \frac{V_e}{a_j^*} \sin \phi \right) P_1}{\left[(1+\beta) (P_2 - P_1) + (1+\beta-\alpha) P_1 \right]} \quad (1)$$

where $\beta = \beta' \gamma M_2^2 / \left(1 + \frac{\gamma-1}{2} M_2^2 \right)$ (2)

$\alpha = P_4/P_1$ (3)

It is suggested² that values of $\beta' = 0.062$ and $\alpha = 1.2$ give good agreement with jet interaction force data. A study was conducted to determine the sensitivity of the jet penetration height (and hence the boundary layer separation distance) to the empirical parameter, β' . The sensitivity of the computed boundary layer separation distance to different values of β' for different nozzle configurations, and test data³, is presented in figure 3.

It was also found that the value of $\beta' = 0.062$ gives adequate agreement with centerline reattachment pressure of Maurer⁴. The reattachment pressure² is:

$$P_R = \left[1 + \beta' \frac{\gamma M_2^2}{1 + \left[(\gamma - 1)/2 \right] M_2^2} \right] P_2 = \left[1 + \beta \right] P_2 \quad (4)$$

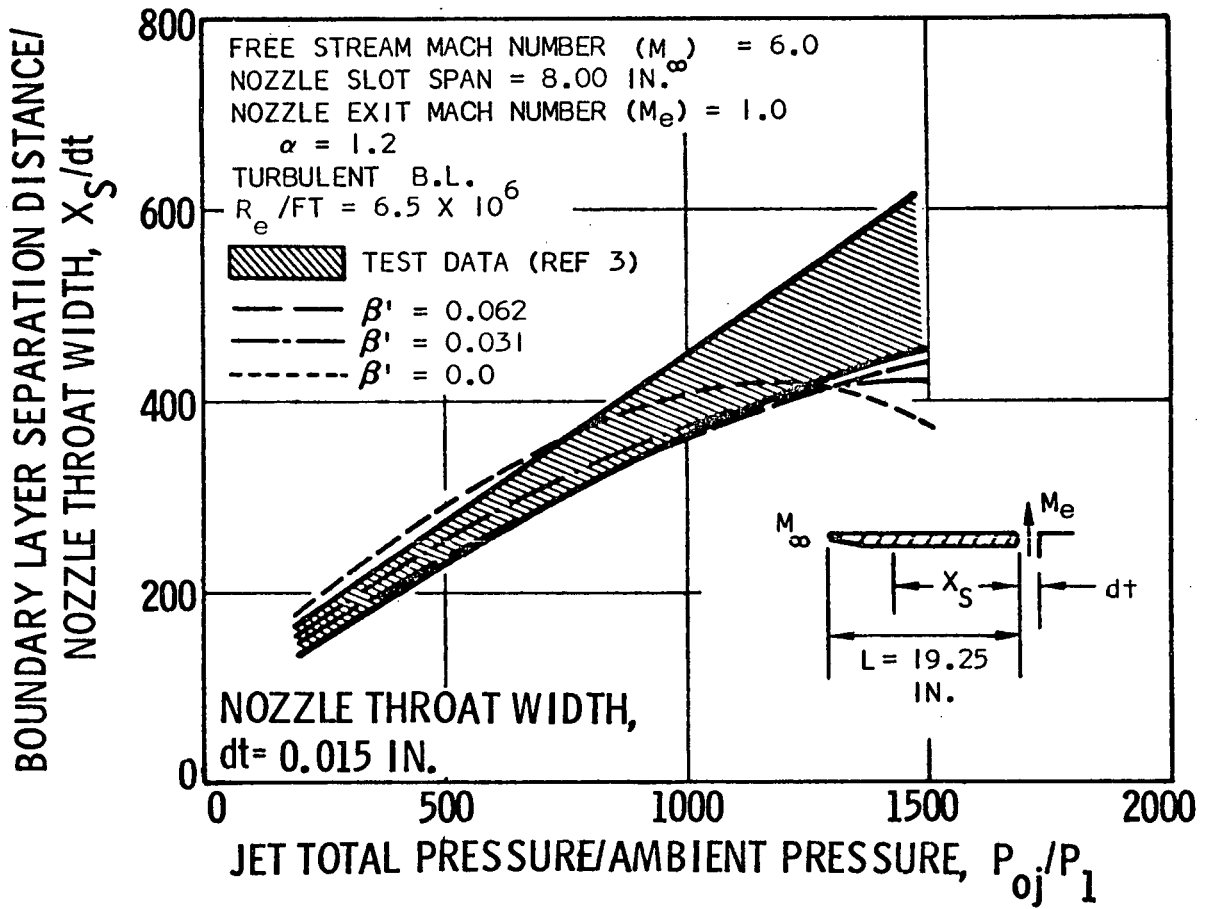


Figure 3 Boundary Layer Separation Distance vs. Pressure Ratio

Three-Dimensional Flow Field Model

When flow begins around the slot ends, slot span flow occurs, and an aspect ratio effect upon jet interaction performance is apparent. Treatment of slot span flow was first suggested by Maurer⁴ by integrating the flow from the centerline of the slot to the slot end, as shown in figure 4. To start the computation procedure, a separation distance (X_s/L) at the centerline (distance the flow separates ahead of the jet) for two-dimensional flow is computed. This distance depends on the local flow, laminar or turbulent, Reynolds number (R_n), the Mach number (M_1), the slot half span to width ratio (b/dt), the ratio of specific heat (γ), and the given jet pressure ratio P_{oj}/P_1 . Estimates of slot span flow are made using the techniques of Maurer, and new separation distances (X) are computed along the slot span. Maurer's oil-film photographs⁴ show, except for the case of a large aspect ratio slot and small jet pressure ratios, the separation line to be elliptic. In this case, the nozzle slot itself is parallel to and in the vicinity of the major axis of the ellipse. The jet penetration height (h_y), figure 4, is therefore assumed to be elliptical when slot span flow is present.

A cross flow parameter,

$$\epsilon = \frac{dQ_s}{h_{(y)} \rho_1 V_1 dy} \quad 0 \leq \epsilon \leq 1.0 \quad (5)$$

specifies a fraction of mass flow $dy h_{(y)} \rho_1 V_1$ entering the control volume surface (1), figure 4, which does not exit through surface (2) after deflection at the separated flow wedge, but spills out the sides of the control volume as dQ_s , figure 4. Thus, in each

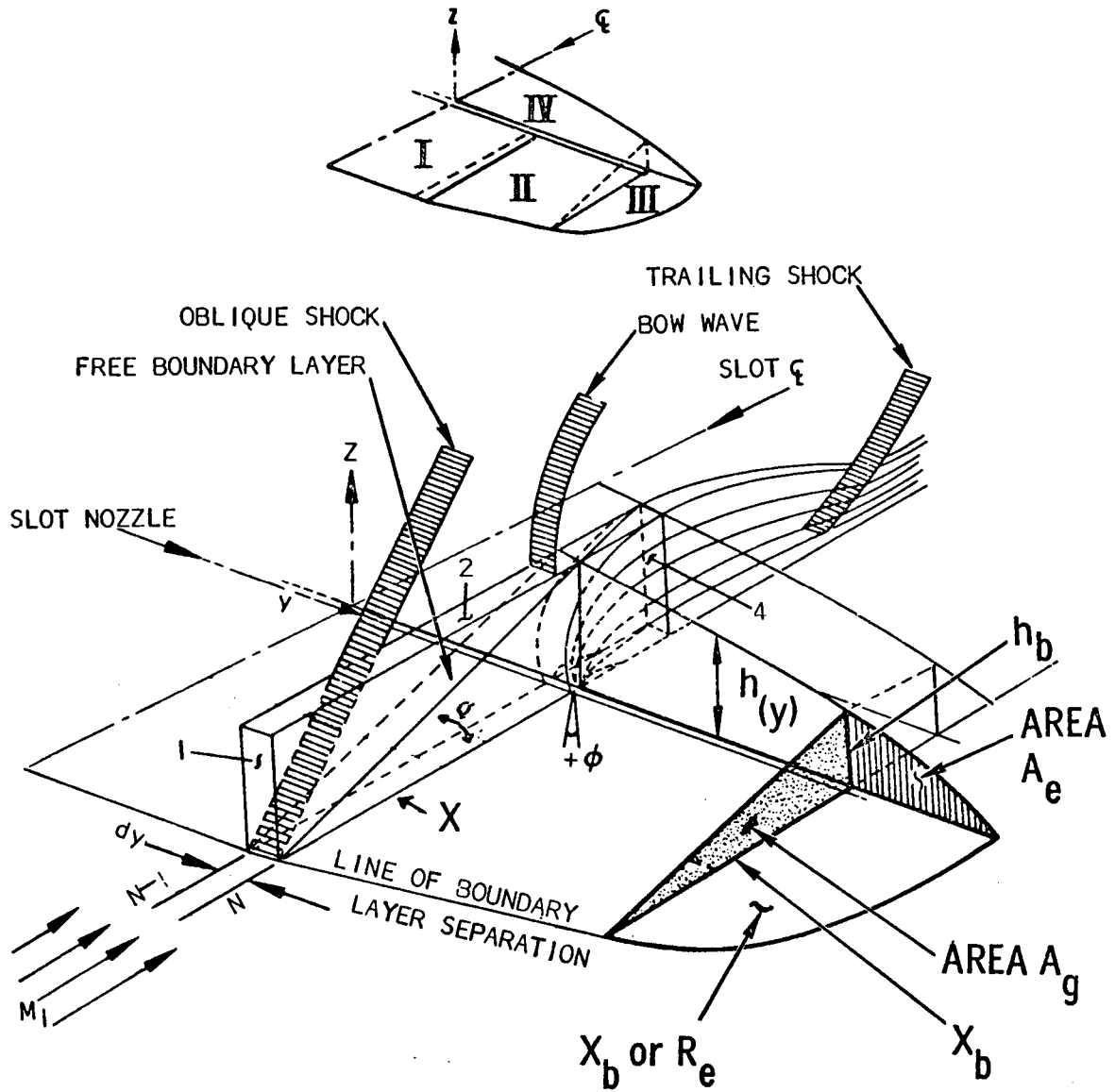


Figure 4 Control Volume

section dy , there exists a cross-stream flux fed by a part of the main stream which entered the control volume.

All freestream flow along the slot centerline shown in figure 4 is initially assumed to be two-dimensional (cross flow $\epsilon_0 = 0$). For the three-dimensional solution, the cross flow parameter ϵ_b is determined at the end of the slot span such that the penetration ellipse equation is satisfied. An iterative solution is used for the ellipse equation

$$1 - (h_b/h_0)^2 = 1/(1 + h_b/(b \tan \sigma))^2 \quad (6)$$

such that for the given value of ϵ_0 the penetration height of the slot centerline is calculated. A search is then conducted to determine ϵ_b which solves the above equation. For each guessed value of ϵ_b the penetration height at the slot span (h_b) and the separated flow or wedge angle (σ_b) is calculated. The program then increments the cross flow parameter (ϵ) between the initial value at the slot centerline ($\epsilon_0 = 0$) and the value determined at the slot end (ϵ_b). The details of this step increment are such that each value of ϵ is related to a distance along the slot span (y) by the penetration ellipse equation. Thus, relatively large dy increments will exist near the center of the flow field where the slot span flow is negligible (approximately two-dimensional) and small where the cross flow is significant.

The difference between the freestream mass flux entering the control volume surface (1), figure 4, and the mass flux over the penetrating jet through surface (2) must equal the lateral flow component dQ_s .

Thus,
$$\epsilon \rho_1 V_1 h_o = \rho_2 V_2 (h_o - h_s) \cos \sigma \tag{7}$$

The ratio h_s/h_o may be derived from equation (7) and a momentum balance across the oblique separation shock, thus

$$\frac{h_s}{h_o} = 1 - \epsilon \frac{\rho_1}{\rho_2} \left\{ \frac{1}{\left[1 - \left(\frac{p_2 - p_1}{2q_1} \right) \right]} \right\} \tag{8}$$

Finally, the product of equations (1) and (8) provides the new penetration height (hs) that when divided by $\tan \sigma$ will define a new separation distance in front of the slot (X_s). The two-dimensional separation and penetration distance is then modified by the lateral cross flow at N along the slot span. In all cases, the slot span flow is redefined until a sonic slot span flow condition exists at the end of the slot. This is accomplished by the computer in the following manner. The geometric area (Ag), figure 4, formed by the penetration height (h_p) and the separated flow distance in front of the slot (X_p) is checked against the choked flow area (A*) associated with the fraction of mass diverted back into the separated region.

$$A_g = \frac{h_b X_b}{2} \quad (9)$$

If A_g equals A^* at the slot span, then the three-dimensional solution has been obtained. If A^* is less than A_g , then the cross flow parameter at the centerline (ϵ_o) is increased until A^* equals A_g . If A^* is greater than A_g , a two-dimensional flow exists in the center section of the slot span and a new slot semi-span (BA) (see figure 2) is computed whose centerline value is $\epsilon_{2d} = 0$.

End Flow Models

The proposed mathematical model treated the flow ahead of the slot from its centerline out to the end of the slot, Sections I and II, (see figure 2). That portion of the freestream that does not pass over the slot jet is diverted outbound in front of the slot, creating slot span flow. Region III (see figure 2) remains to be defined and extends beyond the end of the slot.

Maurer⁴ proposes swinging a radius equal to the separation distance at the slot span for estimates of forces beyond the slot end. The end flow equation in the computer parametric studies used this technique and is as follows:

$$FUE = \frac{\pi L}{4b} \left(\frac{X_b}{L} \right)^2 \left(\frac{P_2 - P_1}{q_1} \right) \quad (10)$$

Little is known about the end flow of a slot^{1, 4} and it is not intended at this time to precisely describe the flow, but to propose a different model suitable for refinement when experimental data becomes available. Nunn⁵ and Karamcheti⁶ propose a blast wave solution for a round jet on a flat plate or on the side of a nozzle. In this analysis the slot span flow at the end of the slot is analogous to the jet on a plate or the side of a rocket nozzle, and the blast wave method defines the slot span flow penetration into the freestream. This penetration distance (R_e) when traced on the surface adjacent to the slot end, is then the separation distance with respect to the slot end.

$$R_e = \left(\frac{4}{\pi} \frac{\gamma}{J} \frac{m_i}{m_o} A_\infty \right)^{1/4} \left(X_e \right)^{1/2} \quad (11)$$

The radius is then computed along the side of the slot to the point where the slot span flow (dQ_g) has been expanded isentropically from sonic conditions at the end of the slot to the freestream Mach number M_1 (see figure 4). The pressure in Region III, Figure 4, is assumed to be the plateau pressure (P_b) Region II at the slot end, decaying to freestream at the line of boundary layer separation. The pressure distribution and resulting cross-sectional area (A_e) is assumed to be that of the

extended penetration ellipse. The following integration is then made over the surface area beyond the slot end for the force:

$$FUE = \int_0^{X_e} \frac{(P_2 - P_1)}{q_1 bL} dA \quad (12)$$

which, when pressure-area terms are included and integration completed, is:

$$FUE = \frac{1}{\pi} \left(\frac{16}{15} \right) \left(\frac{A_e}{L^2} \right) \left(\frac{P_2 - P_1}{q_1 b} \right) \frac{L}{\tan \sigma} \left[\frac{1 - (X_s/X_e)^{5/2}}{1 - (X_s/X_e)} \right] \cos \delta \cos \theta \quad (13)$$

The above technique will allow adjustment of the pressures over the areas affected, the shape of the penetration ellipse, and provide a first real approximation of the flow separation distance beyond the end of the slot.

Surface Curvature Approximation

The necessity of considering the effects of surface curvature on amplification factors are the result of practical applications of a jet steering system. Nunn⁵ estimates the effects of body curvature for orifice amplification factors using a blast wave analogy to the problem. A method has been devised here for the slot jet with slot span flow. The analysis is proposed as a method for extending the effects of body curvature from an orifice to slot jets with slot span flow.

The total force (FU) upstream of the slot is derived by integrating the flat plate component force (FN) for each strip shown in figure 4. For conical or cylindrical bodies, the average component force normal to the x, y plane is computed prior to integration as follows:

$$F_U = \sum_{N=1}^i F_N \cos \delta \cos \theta \quad (14)$$

The force (FUE) at the end of the slot may be corrected in a similar manner for body curvature by using the technique proposed by Nunn.⁵

Finally, the total amplification factor (K_T) is computed and represents a vector normal to the x, y plane.

$$K_T = \frac{F_U + F_{UE} + F_J \cos \phi \cos \delta \cos \theta}{F_{JO}} \quad (15)$$

Comparison to Maurer's Test Data

The experimental data of Maurer⁴ has been replotted and the amplification factors adjusted to use slot jet coefficients referenced to a vacuum. Maurer is not exactly clear about his reference thrust. On the one hand, he refers to the reference slot jet as one coming from a real nozzle, but also implies that his amplification factors (C_n) are referenced to nozzle characteristics of a jet exhausting into an atmosphere rather than a vacuum. The following equation was derived from ideal nozzle equations and used to adjust Maurer's experimental amplification factors to a vacuum reference.

$$\frac{C_n \text{ (Maurer)}}{K \text{ (Vac Ref)}} = \frac{\gamma + 1/\gamma}{V_e/a^*_j} \quad (16)$$

The nozzle exit velocity to throat velocity, V_e/a^*_j , is a function of jet chamber pressure and can be read directly from compressible flow tables⁷, with this, the conversion is easily accomplished.

Figure 5 shows the comparison of Maurer's test data (symbols) and the computer program results at the centerline with no end effect. Maurer's test data are based on centerline integrated pressures for amplification factors, and because of this, no end effects can be evaluated using his experimental data. The tendency to under predict the amplification factors at high jet pressure ratios is evident. Further refinement of the mathematical model to better predict separation pressures at low Mach numbers

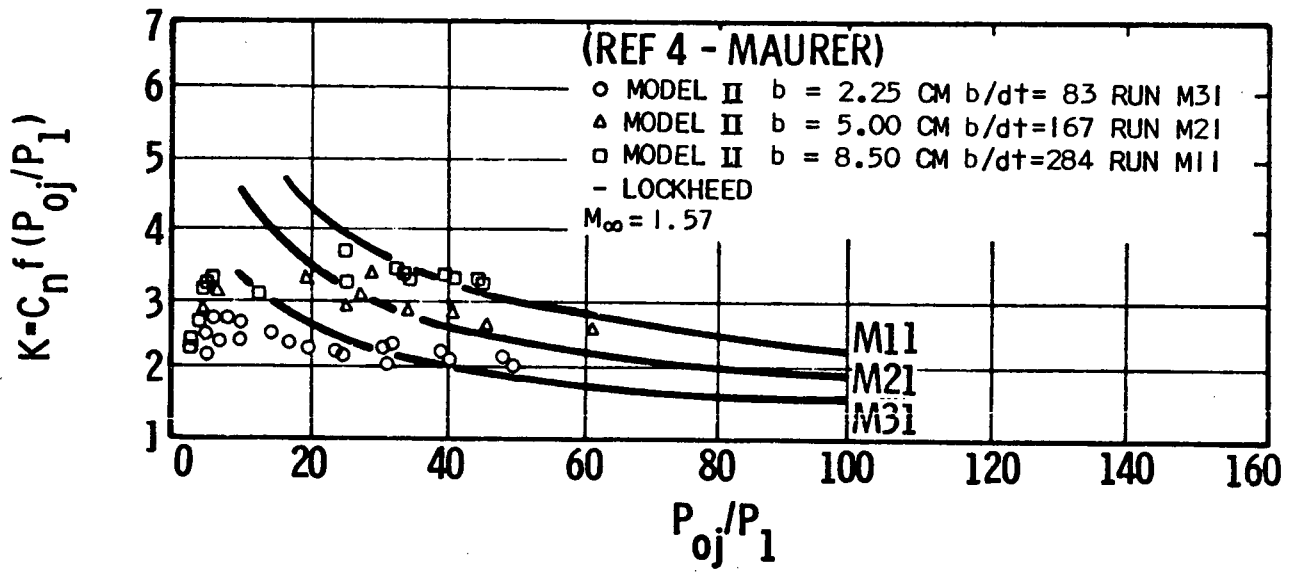


Figure 5 Maurer, Mach 1.57 Comparisons

should improve this trend. When applying a jet interaction control system to a real time trajectory, it was found that low Mach numbers are usually associated with low altitude flight and low chamber pressure ratios. In light of this fact, the dropoff of predicted amplification factors at high jet pressure ratios may not be as important to control system studies as it may first appear.

Comparison To Romeo's Test Data

Romeo's experimental data⁸ were obtained for a slot jet transverse to a Mach 6 freestream flow on a flat plate. Pressure taps were located ahead, to the side of, and in back of the slot. These pressures were integrated over the plate and compared to the thrust of the jet with no flow. Amplification factors are not given, however, the normal force coefficient for the integrated pressures ahead of the jet and the normal force coefficient of the jet were shown. The following equation was derived from the ideal gas equations for a sonic nozzle to convert the data of Romeo to amplification factors:

$$K = \left(\frac{C_{N, A}}{C_{N, R}} + 1 \right) \left(1 - \frac{1}{C_{f_o}} \cdot \frac{P_1}{P_{oj}} \right) \quad (17)$$

Figure 6 presents a comparison of the present analysis with the test data of Romeo. A reasonable correlation was found for the variables investigated. A closer correlation may have been found by adjusting the high Mach number constants (β or α) used in the separation characteristics. The sensitivity of one of these factors was explored and presented in the Spaid and Zukoski model² for separation.

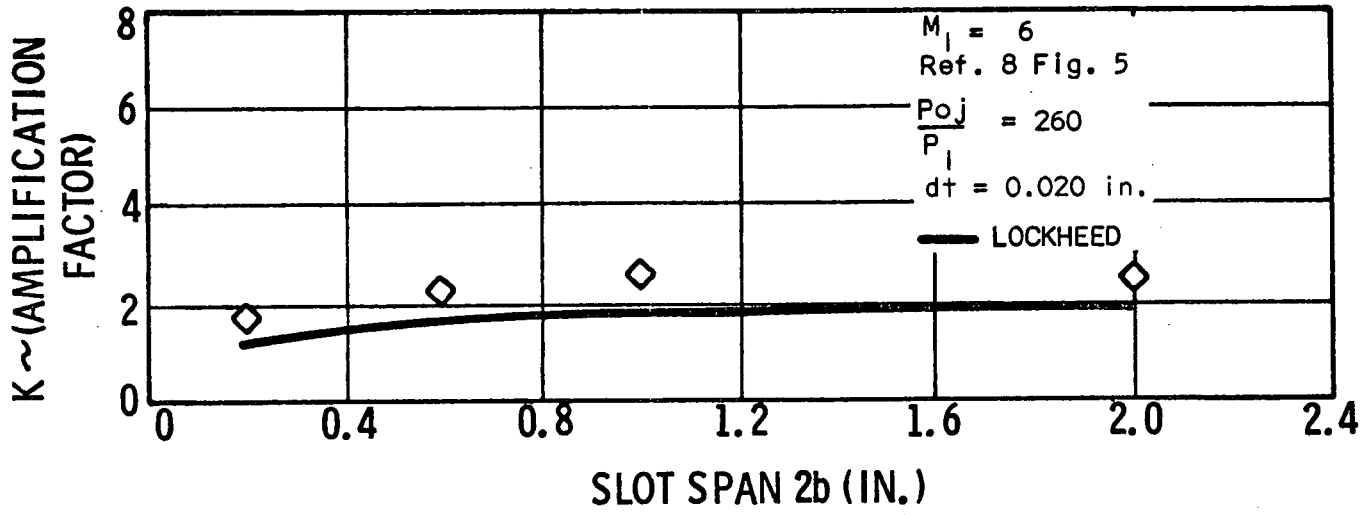


Figure 6 Romeo, Mach 6 Comparisons

Speculation of test equipment problems in the experiments that Romeo conducted comes from the dramatic rise and fall in the amplification factor for small throat widths (dt). Sterrett³ also noted this effect. It is probable that for the small slot widths and high jet pressures, the slot was significantly distorted. If this occurred, the jet may have been tilted forward into the stream with an unknown increased slot width and basic jet thrust change. The construction of the slot in the test rig was such that the back edge of the slot was the edge of a thin flat plate. When this plate bulges due to high jet chamber pressures, the slot would appear to be aimed forward (see Reference 8 for test rig details). Then, as demonstrated by Maurer⁴, where the slot was aimed into the stream, the amplification factor increased substantially. Because of this uncertainty, the test data at throat widths of 5×10^{-3} inches or less are not shown.

Jet Interaction Computer Studies

The jet interaction computer program used for this study uses the method of Barnes combined with Maurer's slot span flow and Spaid and Zukoski separation techniques as described in the preceding comparisons. End effects were estimated using a radius at the slot end. No computer capacity limitations were experienced during any of the studies, including the parametric studies, although many thousands of data points were retained for cross plotting.

The computer run parametric study has been included for demonstration purposes. It is typical of a slot jet application to a low altitude (atmospheric) supersonic missile. Two types of information were plotted, (1) data used for engineering evaluation of the method employed, and (2) data for systems evaluation when conducting preliminary

design studies. The following were the basic input values for this parametric study:

Slot jet assumed to be installed on a flat surface.

γ	1.4 freestream
γ_j	1.25 nozzle
$\frac{V_e}{a_j^*}$	1.805 velocity at exit of nozzle to throat
$\frac{P_{oj}}{P_1}$	40-100 chamber pressure to freestream static
M_1	2 to 6.6
$\frac{b}{dt}$	10 to 90 aspect ratio
$\frac{dt}{L}$	0.00288 throat diameter to reference length
$\frac{b}{L}$	0.00144→0.131 half span to reference length
T_1	900°R freestream temperature
ϕ	39° nozzle pointed forward from vertical
$R_n = 1 \times 10^7$	Local Reynolds number at nozzle, turbulent

Figures 7 thru 10 present the results of the parametric study for engineering use. Amplification factors for the slot span are integrated values along the span with a quarter circle radius at the ends for end effects. Centerline amplification factors are shown by assuming centerline conditions existing uniformly over the slot span with a radius at the slot end for end effects. For information, two-dimensional values with no end effects are shown. X_g is the separation distance ahead of the slot referenced to the distance from the origin of the boundary layer to the slot. h_g/h is the ratio of the separation height at the slot (with slot span flow) to the separation height if no slot span flow existed. P_R/P_1 is the ratio of reattachment pressure to local freestream pressure ratio.

Figure 11 is a plot of amplification factors for a slot with end effects as a function of aspect ratio, Mach number, and chamber pressure. The forces a slot jet system can produce with respect to a slot exhausting to a vacuum can be computed using the amplification factors presented. For example, $\gamma = 1.4$, $P_{oj}/P_1 = 80$, Mach number = 4 and b/dt of 10, Figure 11 shows K_T equal to 2.25. The control force is then $F_U + F_{JO} = 2.25 C_{fo} \cdot P_{oj} \cdot dt$, where:

$$C_{fo} = (\gamma + 1) \left(\frac{2}{\gamma + 1} \right)^{\left(\frac{\gamma}{\gamma - 1} \right)} = 1.268 \quad (18)$$

From the figures, increased aspect ratio and Mach number show increases in amplification factor. Conversely, as jet pressure ratios increased, amplification factors decreased. The time required on the IBM 1108 computer to conduct this study was five minutes including the plotting. A new parametric can be set up for the computer in about two hours.

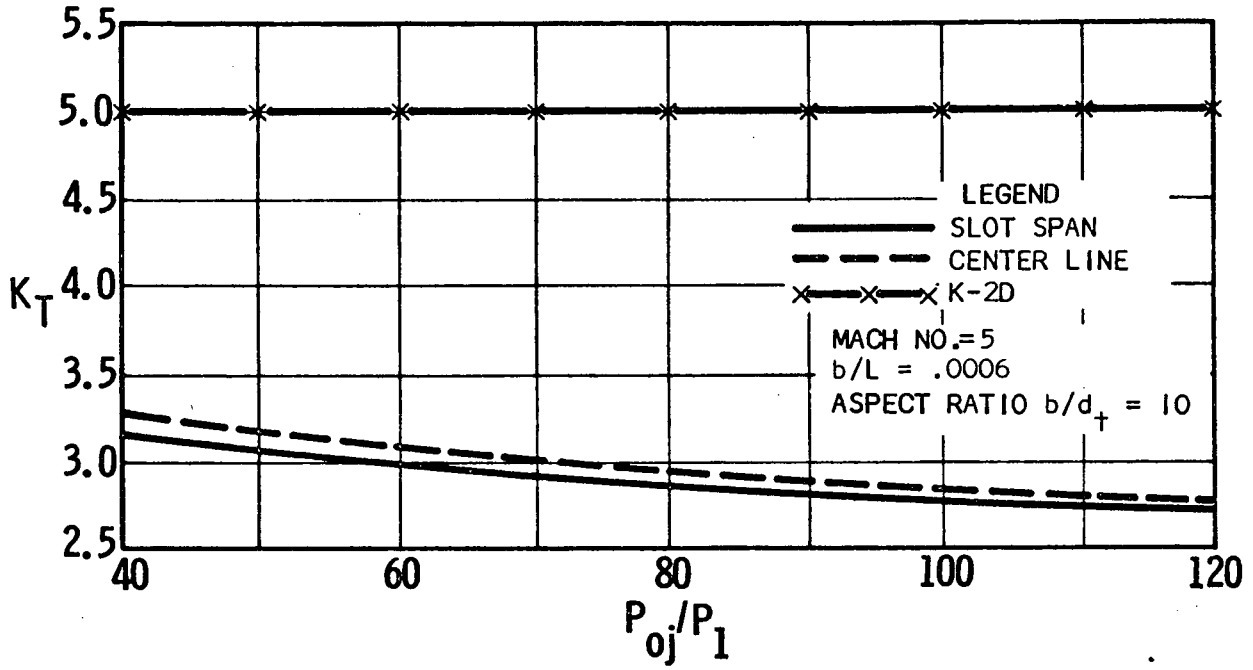


Figure 7 Amplification Factor Vs Jet Pressure Ratio

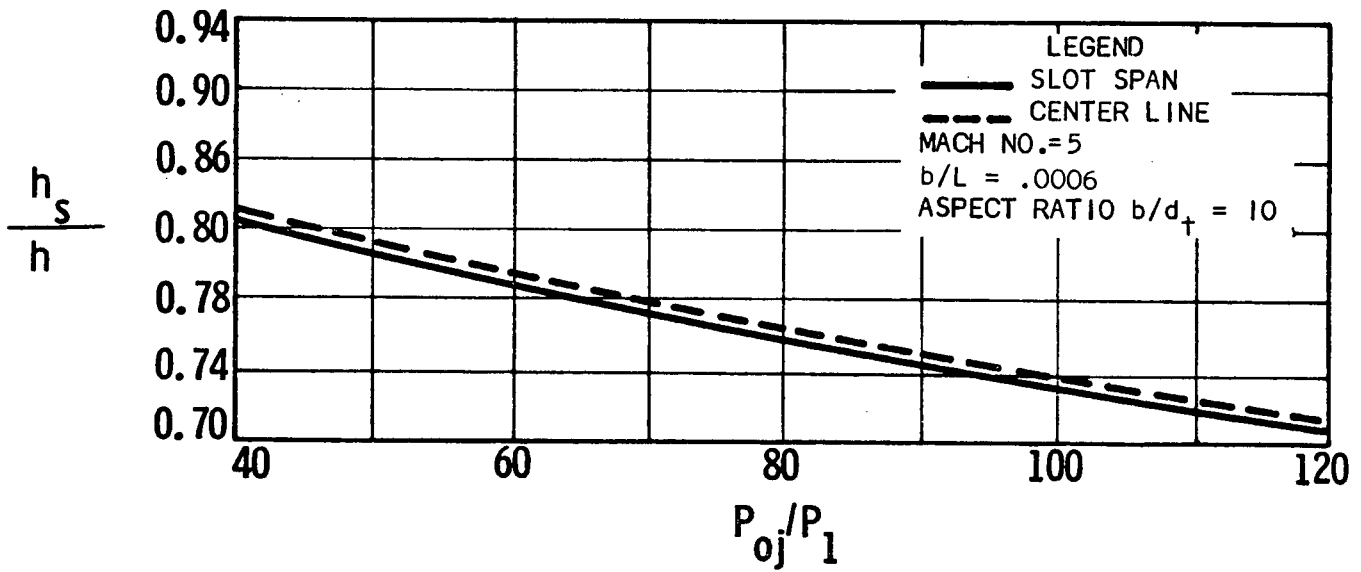


Figure 8 Penetration Height Vs Jet Pressure Ratio

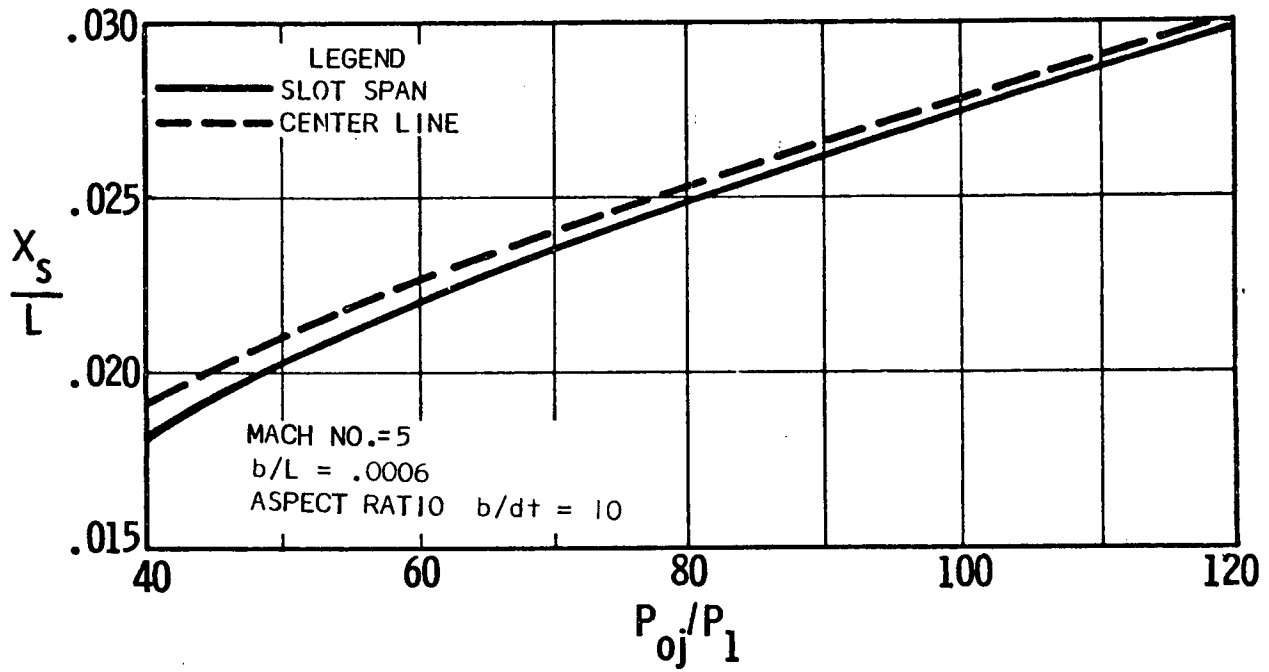


Figure 9 Separation Distance Vs Jet Pressure Ratio

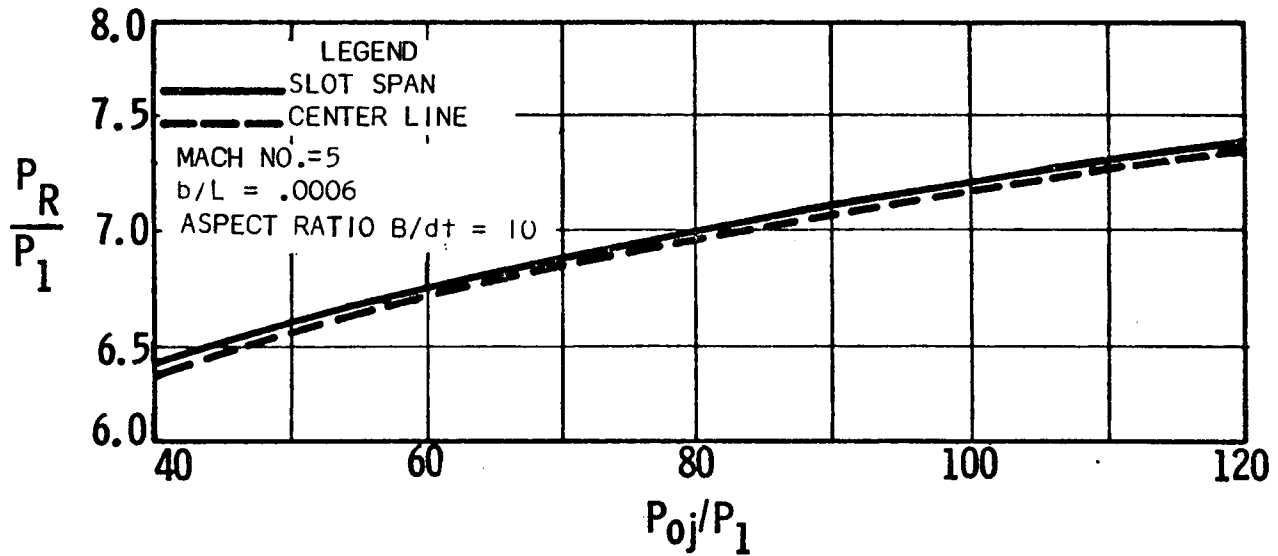


Figure 10 Reattachment Pressure Vs Jet Pressure Ratio

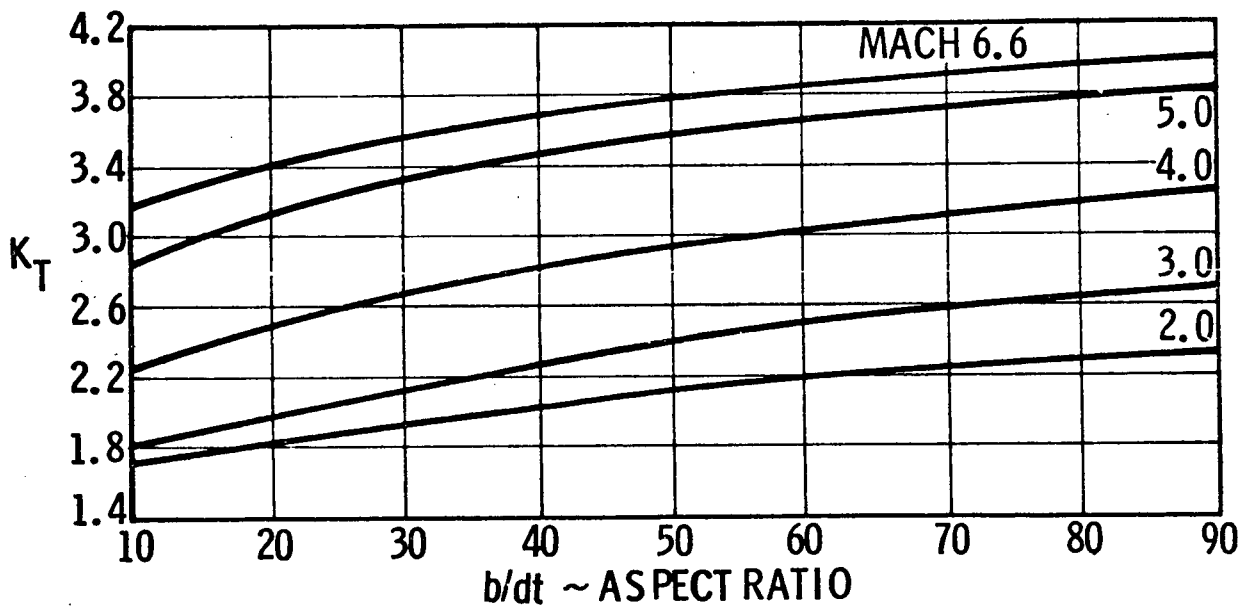


Figure 11 Computer Parametric, P_{o_j}/P_1 Equal 80

Conclusions

- A large number of jet interaction variables were evaluated and the amplification factors computed show reasonable agreement with experimental data.
- The empirical constants, $\beta = 0.062$ and $\alpha = 1.2$, of equations (2), (3) were found to provide adequate agreement with centerline pressures and boundary layer separation distance estimates. These constants were then used in the basic momentum balance to determine the jet penetration height.
- Slot span flow greatly affects the prediction of amplification factor for low aspect ratio slots at a significantly high jet-to-freestream pressure ratio.
- Slot span end flow greatly increases the prediction of total amplification factor. The end flow surface area has been approximated by swinging a radius (quarter circle) equal to the separation distance at the end of the slot. The blast wave theory is proposed for the small aspect ratio slots at significantly high pressure ratios.
- Total amplification factor is reduced by body curvature. Predicted amplification factors can be estimated by correcting the differential force increment for the warped surface prior to integration.
- The three-dimensional model developed enables future parametric study to include the effects of viscous mixing in the separation and penetration mixing regions, and provides the flow conditions necessary for the prediction of downstream effects.

Recommendations

- Incorporate a viscous modeling technique such that the amount of freestream-jet mixing in the separated region can be estimated.
- Model the downstream flow field specifically to determine the reattachment region distance from the slot.
- Complete a study of pressure distribution on the immediate aft side of the jet using a method dependent on freestream and flow conditions above the jet.
- Define a technique and estimate the effects of jet interaction with burning (JIB) on the amplification factor. Both the upstream and downstream regions should be considered using a reactive gas jet.

References

1. Barnes, J. W., et al, "Control Effectiveness of Transverse Jets Interacting with a High-Speed Free Stream," Vol. 1, AFFDL TR 67-90, Sept. 1967 (U).
2. Spaid, F. W. and Zukoski, E., "A Study of the Interaction of Gaseous Jets from Transverse Slots with Supersonic External Flows," AIAA Vol. 6, No. 2, Feb. 1968 (U).
3. Sterrett, J. R., et al, "Experimental Investigation of Secondary Jets From Two-Dimensional Nozzles with Various Exit Mach Numbers for Hypersonic Control Application," NASA TN-D-3795, Jan. 1967 (U).
4. Maurer, F., "Interference Effects Produced by Gaseous Side-Jets Issuing Into a Supersonic Stream", TG 230-T460, 22 Nov. 1965. (U)
5. Nunn, R. H., "Jet Interaction Wrap-Around on Bodies of Revolution," AIAA Vol. 7, No. 3, March 1970 (U).
6. Karamcheti, K., et al, "Integral Approach to an Approximate Analysis of Thrust Vector Control by Secondary Injection," AIAA Vol. 1, No. 11, Nov. 1969 (U).
7. Ames Research Staff, "Equation Tables and Charts for Compressible Flow," NACA TN 1135, 1953 (U).
8. Romeo, D. J., "Aerodynamic Interaction Effects Ahead of Rectangular Sonic Jets Exhausting Perpendicularly From a Flat Plate into a Mach Number 6 Free Stream," NASA TND-1800, May 1963 (U).
9. Culp, M. F., "Interceptor Vehicle Aerodynamics and Controls, Revision A" LMSC D130505A, 1969 Independent Development Program (U).

Appendix B

USER'S MANUAL FOR THE THRUST VECTOR
CONTROL PERFORMANCE PROGRAM

B-1

Appendix B

A detailed description of the program input instructions follows:

- Detailed Input Guide
- Sample Program Input
- Sample Program Output.

Card 1

Format 7E10.5

<u>Column</u>	<u>Parameter</u>	<u>Definition</u>
1-10	SPR	secondary-to-primary total pressure ratio
11-20	XL	ratio of distance from primary nozzle throat to the injection point divided by nozzle length
21-30	EPS	secondary injection angle (deg)
31-40	SM	secondary injection Mach number
41-50	CMS	secondary nozzle flow coefficient
51-60	VNS	secondary vacuum momentum specific impulse efficiency
61-70	PTP	primary total pressure (psfa)

Card 2

Format 7E10.5

1-10	ARATIO	primary nozzle area ratio
11-20	GAMS	ratio of specific heats for the secondary gas
21-30	VNP	primary vacuum momentum specific impulse efficiency

B-1-a

<u>Column</u>	<u>Parameter</u>	<u>Description</u>
31-40	CDP	primary nozzle flow coefficient
41-50	SMI	initial secondary mass flow ratio
51-60	PSL	local static pressure (psfa)

Card 3

Format 6E10.5

1-10	WMP	primary gas molecular weight
11-20	WMS	secondary gas molecular weight
21-30	TTP	primary gas total temperature ($^{\circ}$ R)
41-50	WPRI	primary mass flow rate

Card 4

Format 7E10.5

1-10	TTS	secondary gas molecular weight ($^{\circ}$ R)
11-20	GAMP	ratio of the specific heats of the primary gas
21-30	PM	local primary flow Mach number
31-40	S	interaction distance (ft)
41-50	AS	secondary flow area (ft ²)

Card 5

Format 5E10.5

1-10	CFP	primary nozzle thrust coefficient
11-20	ALPHA	nozzle divergence angle (deg)
21-30	SMINC	secondary mass flow increment
31-40	SMMAX	maximum secondary mass flow

SAMPLE PROGRAM INPUT

DATA	IL	CHUC	FINI							
DATA PROCESSOR LEVEL 3										
000001	MAP, IL A, A									
000002	LIB SYSS, MSFCS,									
000003	XQT A									
000004	.9	.25	75.	1.	.93	.965	100800.			
000005	7.	1.15	.9768	.99	.02	13225.				
000006	20.	20.	1500.	100.						
000007	1500.	1.15	2.011	.326	.000729626					
000008	1.51	15.0	.02	.29						
000009	XQT A									
000010	.9	.25	60.	1.	.93	.965	100800.			
000011	7.	1.15	.9768	.99	.02	13225.				
000012	20.	20.	1500.	100.						
000013	1500.	1.15	2.011	.326	.000729626					
000014	1.51	15.0	.02	.29						
000015	XQT A									
000016	.9	.25	45.	1.	.93	.965	100800.			
000017	7.	1.15	.9768	.99	.02	13225.				
000018	20.	20.	1500.	100.						
000019	1500.	1.15	2.011	.326	.000729626					
000020	1.51	15.0	.02	.29						
000021	XQT A									
000022	.9	.5	75.	1.	.93	.965	100800.			
000023	7.	1.15	.9768	.99	.02	6350.				
000024	20.	20.	1500.	100.						
000025	1500.	1.15	2.405	.2171	.000729626					
000026	1.51	15.0	.02	.29						
000027	XQT A									
000028	.9	.5	60.	1.	.93	.965	100800.			
000029	7.	1.15	.9768	.99	.02	6350.				
000030	20.	20.	1500.	100.						
000031	1500.	1.15	2.405	.2171	.000729626					
000032	1.51	15.0	.02	.29						
000033	XQT A									
000034	.9	.5	45.	1.	.93	.965	100800.			
000035	7.	1.15	.9768	.99	.02	6350.				
000036	20.	20.	1500.	100.						
000037	1500.	1.15	2.405	.2171	.000729626					
000038	1.51	15.0	.02	.29						
000039	XQT A									
000040	.9	.75	75.	1.	.93	.965	100800.			
000041	7.	1.15	.9768	.99	.02	365.6				
000042	20.	20.	1500.	100.						
000043	1500.	1.15	2.680	.1083	.000729626					
000044	1.51	15.0	.02	.29						
000045	XQT A									
000046	.9	.75	60.	1.	.93	.965	100800.			
000047	7.	1.15	.9768	.99	.02	365.6				
000048	20.	20.	1500.	100.						
000049	1500.	1.15	2.680	.1083	.000729626					
000050	1.51	15.0	.02	.29						
000051	XQT A									
000052	.9	.75	45.	1.	.93	.965	100800.			
000053	7.	1.15	.9768	.99	.02	365.6				
000054	20.	20.	1500.	100.						
000055	0.	1.15	2.680	.1083	.000729626					
000056	1.51	15.0	.02	.29						

AS	CFMP	CFMN	THET	SMR
7.29626-04	1.00443+00	8.75623-02	1.39806+00	2.00000-02
CFIN1	CFIN2	CFIN	AF	PTS
2.84115+01	8.75706-01	8.75706-01	1.22028+00	4.87742+04
CFX	CFY	CFMX	CFMY	ALPHA
3.14210-01	1.85029+00	8.75612-02	1.00443+00	1.50000+01
FS/FA				
2.44056-02				

SAMPLE PROGRAM OUTPUT

AS	CFMP	CFMN	THET	SMR
7.29626-04	1.14275+00	1.24627-01	2.98773+00	4.00000-02
CFIN1	CFIN2	CFIN	AF	PTS
1.42057+01	8.75706-01	8.75706-01	1.30483+00	9.75484+04
CFX	CFY	CFMX	CFMY	ALPHA
3.51275-01	1.98862+00	1.24626-01	1.14275+00	1.50000+01
FS/FA				
5.21930-02				

LMSC-HREC D306359

B-4

Appendix C
LISTING OF THE TVC PERFORMANCE
COMPUTER PROGRAM

C-1

MAIN PROGRAM

STORAGE USED: CODE(1) 001251; DATA(0) 000242; BLANK COMMON(2) 000000

EXTERNAL REFERENCES (BLOCK, NAME)

0003 NINTRS
 0004 NRDU5
 0005 NI025
 0006 NEXP65
 0007 SWRT
 0010 TAN
 0011 CUS
 0012 SIR
 0013 ATAN
 0014 NRDU5
 0015 NSTOPS

STORAGE ASSIGNMENT (BLOCK, TYPE, RELATIVE LOCATION, NAME)

0000	000162	10F	0001	000071	100L	0001	001245	101L	0001	000325	111L	0001	000400	112L
0000	000164	12F	0000	000166	14F	0000	000170	16F	0000	000172	18F	0000	000116	200F
0000	000130	201F	0000	000133	202F	0000	000145	203F	0000	000157	204F	0000	R	000060
0000	R	000112	AF	0000	R	000030	ALPHA	0000	R	000053	AP	0000	R	000010
0000	R	000047	ASEFF	0000	R	000054	ASTARP	0000	R	000061	B	0000	R	000062
0000	R	000102	CFIN	0000	R	000075	CFINI	0000	R	000100	CFIN2	0000	R	000103
0000	R	000083	CFMN	0000	R	000057	CFMP	0000	R	000106	CFMX	0000	R	000107
0000	R	000041	CFVO	0000	R	000110	CFX	0000	R	000111	CFY	0000	R	000036
0000	R	000005	CHS	0000	R	000037	CSTARP	0000	R	000040	CSTAR5	0000	R	000056
0000	R	000065	E	0000	R	000003	EPS	0000	R	000066	F	0000	R	000067
0000	R	000011	GAMS	0000	R	000114	GIMANG	0000	R	000071	H	0000	I	000034
0000	R	000072	P	0000	R	000101	PED	0000	R	000024	PH	0000	R	000015
0000	R	000043	PTS	0000	R	000076	Q	0000	R	000105	R	0000	R	000025
0000	R	000014	SMI	0000	R	000031	SHINC	0000	R	000032	SHMAX	0000	R	000033
0000	R	000113	T	0000	R	000044	TERMI	0000	R	000045	TERM2	0000	R	000046
0000	R	000051	TERM5	0000	R	000052	TERM6	0000	R	000115	THETAG	0000	R	000020
0000	R	000064	TU	0000	R	000012	VNP	0000	R	000006	VNS	0000	R	000074
0000	R	000017	WMS	0000	R	000021	WPRI	0000	R	000042	WSEC	0000	R	000070
0000	R	000077	W3	0000	R	000002	XL					0000	R	000073

- 1. C
- 2. C
- 3. C
- 4. C
- 5. C
- 6. C
- 7. C

*** INPUT PARAMETERS ***

AF = AMPLIFICATION FACTOR
 ALPHA = PRIMARY NOZZLE LOCAL WALL ANGLE (DEGREES)
 ARATIO = PRIMARY NOZZLE AREA RATIO
 AS = SECONDARY GEOMETRICAL FLOW AREA (SQUARE FEET)
 ASEFF = EFFECTIVE SECONDARY FLOW AREA (SQUARE FEET)

00100	8.	C	ASTANK=PRIMARY NOZZLE THROAT AREA (SQURE FEET)
00100	9.	C	CDP = PRIMARY NOZZLE FLOW COEFFICIENT
00100	10.	C	CFIN= MINIMUM VALUE OF CFIN1 OR CFIN2
00100	11.	C	CFIN1 = HIGH SECONDARY MASSFLOW INDUCED FORCE COEFFICIENT
00100	12.	C	CFIN2 = LOW SECONDARY MASSFLOW INDUCED FORCE COEFFICIENT
00100	13.	C	CFMN= NORMAL SECONDARY INJECTION MOMENTUM THRUST COEFFICIENT
00100	14.	C	CFMP= PARALLEL SECONDARY INJECTION MOMENTUM THRUST COEFFICIENT
00100	15.	C	CFMX =MOMENTUM THRUST COEF. PARALLEL TO PRIMARY NOZZLE AXIS
00100	16.	C	CFMY =MOMENTUM THRUST COEF. NORMAL TO PRIMARY NOZZLE AXIS
00100	17.	C	CFP = PRIMARY THRUST COEFFICIENT (NO TVC EFFECT)
00100	18.	C	CFVO= ISENTROPIC THRUST COEFFICIENT
00100	19.	C	CFX = SECONDARY THRUST COEFFICIENT PARALLEL TO PRIMARY NOZZLE AXIS
00100	20.	C	CFY = SECONDARY THRUST COEFFICIENT NORMAL TO PRIMARY NOZZLE AXIS
00100	21.	C	CMS = SECONDARY NOZZLE FLOW COEFFICIENT
00100	22.	C	CSTANK=PRIMARY FLOW CHARACTERISTIC VELOCITY (FEET PER SECOND)
00100	23.	C	CSTANK=SECONDARY FLOW CHARACTERISTIC VELOCITY (FEET PER SECOND)
00100	24.	C	DP = DIAMETER OF THE PRIMARY NOZZLE THROAT (FEET)
00100	25.	C	EPS = SECONDARY INJECTION ANGLE (DEGREES)
00100	26.	C	GAMP= PRIMARY RATIO OF SPECIFIC HEATS
00100	27.	C	GAMS= SECONDARY RATIO OF SPECIFIC HEATS
00100	28.	C	GIMANG = GIMBAL ANGLE (RADJANS)
00100	29.	C	PED = PRIMARY EXIT DIAMETER (FEET)
00100	30.	C	PM = LOCAL PRIMARY FLOW MACH NUMBER
00100	31.	C	PSL = PRIMARY NOZZLE LOCAL WALL STATIC PRESSURE (PSFA)
00100	32.	C	PTP = PRIMARY TOTAL PRESSURE (PSFA)
00100	33.	C	PTS = SECONDARY TOTAL PRESSURE (PSFA)
00100	34.	C	S = INTERACTION DISTANCE (FEET)
00100	35.	C	SM = SECONDARY INJECTION MACH NUMBER
00100	36.	C	SMI = INITIAL SECONDARY MASSFLOW RATIO
00100	37.	C	SMINC = SECONDARY MASSFLOW INCREMENT
00100	38.	C	SHMAX = MAXIMUM SECONDARY MASSFLOW
00100	39.	C	SMR = SECONDARY TO PRIMARY MASSFLOW RATE RATIO
00100	40.	C	SPR = SECONDARY TO PRIMARY INJECTION TOTAL PRESSURE RATIO
00100	41.	C	T = SMR*AF
00100	42.	C	THETAG = GIMBAL ANGLE (DEGREES)
00100	43.	C	TIP = PRIMARY TOTAL TEMPERATURE (DEGREES RANKINE)
00100	44.	C	TTS = SECONDARY TOTAL TEMPERATURE (DEGREES RANKINE)
00100	45.	C	TU = BLAST WAVE ACCUMULATION OF TERMS
00100	46.	C	VNP = VACUUM MOMENTUM SPECIFIC IMPULSE EFFICENCY (PRIMARY)
00100	47.	C	VNS = VACUUM MOMENTUM SPECIFIC IMPULSE EFFICENCY (SECONDARY)
00100	48.	C	W = OMEGA
00100	49.	C	W1 = BLAST WAVE OMEGA ONE DIMENSION LESS ENERGY
00100	50.	C	W2 = BLAST WAVE OMEGA TWO DIMENSION LESS ENERGY
00100	51.	C	W3 = BLAST WAVE OMEGA THREE DIMENSIONLESS ENERGY
00100	52.	C	#MP = PRIMARY GAS MOLECULAR WEIGHT
00100	53.	C	#MS = SECONDARY GAS MOLECULAR WEIGHT
00100	54.	C	#PRI= PRIMARY MASSFLOW RATE (POUNDS PER SECOND)
00100	55.	C	#SEC= SECONDARY MASSFLOW RATE (POUNDS PER SECOND)
00100	56.	C	XL = RATIO OF DISTANCE FROM PRIMARY NOZZLE THROAT TO INJECTION POINT
00100	57.	C	DIVIDED BY PRIMARY NOZZLE LENGTH
00100	58.	C	
00101	59.		REAL L
00103	60.		READ(5,10) SPR,XL,EPS,SM,CMS,VNS,PTP
00114	61.		READ(5,12) ARATIO,GAMS,VNP,CDP,SMI,PSL
00124	62.		READ(5,14) #MP,#MS,TTP,#PRI
00132	63.		READ(5,16) TTS,GAMP,PM,S,AS

00141	64.	READ(5,18)CFP,ALPHA,SMINC,SMMAX	
00141	65.		
00141	66.		
00141	67.	C CFMP CALCULATION	010
00141	68.	C	
00147	69.	SMR = SM1 - SMINC	011
00150	70.	ICOUNT = 0	
00151	71.	100 CONTINUE	
00152	72.	ALPHA = ALPHA/57.29582	006
00153	73.	SMR = SMR + SMINC	012
00154	74.	IF(SMR.GT. SMMAX) GO TO 101	014
00156	75.	CGAMS=(GAMS**5)*((2.0/(GAMS+1.))**((GAMS+1.)/(2.*(GAMS-1.)))	020
00157	76.	CGAMP = ((GAMP)**5)*((2.0/(GAMP+1.0))**((GAMP+1.0)/(2.0*(GAMP-1.	024
00157	77.	1)))	025
00160	78.	CSTARP = SQRT((1544.0/WMP)*TTP)/CGAMP	026
00161	79.	CSTARS=SQRT((1544.0/WMS)*TTS)/CGAMS	030
00162	80.	CFV0=(CGAMS)*(1.0+GAMS*SM**2.0)/(SQRT(GAMS))*(SM) *(1.+(GAMS-1.)	040
00162	81.	1/2.0*SM**2.0))**.5	
00163	82.	WSEC=WPR1*SMR	060
00164	83.	*DIAGNOSTIC* THE TEST FOR EQUALITY BETWEEN NON-INTEGERS MAY NOT BE MEANINGFUL.	
00164	83.	IF((AS.NE.0.0) .AND. (ICOUNT.EQ.0)) GO TO 111	
00166	84.	PTS = SPR*PTP	065
00167	85.	TERM1=SQRT(GAMS*WMS/1544.)	076
00170	86.	TERM2=PTS/SQRT(TTS)	077
00171	87.	TERM3=SM/(1.+(GAMS-1.)/2.)*SM*SM**((GAMS+1.)/(2.*(GAMS-1.	078
00171	88.	1)))	079
00172	89.	AS = WSEC/(TERM1*TERM2*TERM3*32.2)	080
00173	90.	ASEFF=AS*CMS	070
00174	91.	ICOUNT = ICOUNT + 1	
00175	92.	GO TO 112	
00176	93.	111 ASEFF = AS*CMS	
00177	94.	TERM1=SQRT(GAMS*WMS/1544.)	
00200	95.	TERM3=SM/(1.+(GAMS-1.)/2.)*SM*SM**((GAMS+1.)/(2.*(GAMS-1.	
00200	96.	1)))	
00201	97.	PTS = (WSEC*SQRT(TTS))/(ASEFF*TERM1*TERM3*32.2)	
00202	98.	112 CONTINUE	
00203	99.	TERM4 = SQRT(GAMP*WMP/1544.)	081
00204	100.	TERM5 = PTP/SQRT(TTP)	082
00205	101.	TERM6 = 1.0/(1.+(GAMP-1.)/2.)*1.)*((GAMP+1.)/(2.*(GAMP-1.	083
00205	102.	1)))	084
00206	103.	AP = WPR1/(TERM4*TERM5*TERM6*32.2)	085
00207	104.	ASTARP = AP*CDP	086
00210	105.	DP = SQRT(4.*ASTARP/3.14159)	087
00211	106.	D=(PSL/PTP)*(1./SMR)*(CSTARP/CSTARS)*((ASEFF)/(CDP*ASTARP))	120
00212	107.	CFMP=(VNS)*(CFV0)-D	110
00212	108.	C	
00212	109.	C CFMN CALCULATION	130
00212	110.	C	
00213	111.	A=(3.14159)*(CGAMS)*((.5)-(EPS/180.0))	140
00214	112.	B=(CMS)*SQRT(GAMS)*SM	150
00215	113.	C=SQRT(1.0+(GAMS-1.0) * (SM**2.0)/(2.0))	160
00216	114.	CFMN=(A/(B*C))-D/TAN(EPS/57.29582)	170
00216	115.	C	
00216	116.	C THEORY 1 INDUCED FORCES (HIGH SMR)	180
00216	117.	C	
00217	118.	TU=(1.175)*(GAMP)-1.05	190

00217	119.			
00217	120.	C	OMEGA CALCULATIONS, OMEGA ONE FIRST	200
00217	121.	C		
00220	122.		$E = (1.0 + (GAMP - 1.0) * ((PM * 2.0) / 2.0))$	210
00221	123.		$F = (CSTARP / CSTAR)$	220
00222	124.		$G = ((5.0 * GAMP) - 3.0) / ((8.0 * GAMP) - 8.0)$	230
00223	125.		$W1 = ((PM * 1.25) * (F * .75)) / (E * G)$	240
00223	126.	C		
00223	127.	C	OMEGA TWO CALCULATIONS	250
00223	128.	C		
00224	129.		$H = (GAMP) * (GAMP - 1.0) * (PM * 2.0)$	260
00225	130.		$P = (GAMS / (GAMS - 1.0))$	270
00226	131.		$W2 = .5 * (1.0 / H) * (P * E) / ((GAMP * PM * 2.0) * ((CGAMS / CGAMP) * 2.0) * (1.0 / F) * 2.0 * (SM / PM) * SQRT(E) / C * (SQRT(GAMS / GAMP)) * (CGAMS / CGAMP) * (1.0 / F) * 2 * COS(EPS / 57.29582))$	280
00226	132.			290
00226	133.			300
00226	134.	C		
00226	135.	C	OMEGA CALCULATION	310
00226	136.	C		
00227	137.		$W = W1 * (W2 * .75)$	320
00227	138.	C		
00227	139.	C	CFIN1 CALCULATION	330
00227	140.	C		
00230	141.		$CFIN1 = (TU) * (W) * (SQRT(S / (SQRT(CDP) * (DP)))) * (1.0 / SMR) * (F * .25)$	340
00230	142.	C		
00230	143.	C	THEORY 2 INDUCED FORCES (LOW SMR)	350
00230	144.	C		
00231	145.		$Q = SQRT(GAMP) * CGAMP * (GAMP - 1.0) * (PM * 3.0)$	360
00231	146.	C		
00231	147.	C	OMEGA THREE CALCULATION	370
00231	148.	C		
00232	149.		$W3 = W2 * ((1.0 / ((GAMP - 1.0) * PM * 2.0)) * (WHP / WMS) * (1.0 - ((GAMP - 1.0) / (GAMS - 1.0)) * GAMS / GAMP) + (GAMP - 1.0) / GAMP + (SM / PM) * (SQRT(E) / C) * SQRT(2 * GAMS / GAMP) * (CGAMS / CGAMP) * (1.0 / F) * COS(EPS / 57.29582))$	380
00232	150.			390
00232	151.			400
00232	152.	C		
00232	153.	C	CFIN2 CALCULATION	410
00232	154.	C		
00233	155.		$CFIN2 = (Q * F * W3) / (((PM * 2.0) - 1.0) * (E)) * .5$	420
00234	156.		$PED = SQRT(ARATIO * DP * 2.0)$	422
00235	157.		$L = 1.0 - .65 * (S / PED) * 1.25$	440
00236	158.		$CFIN1 = .7 * L * CFIN1$	450
00237	159.		$CFIN2 = 1.0 * L * CFIN2$	460
00240	160.		$CFIN = AMIN1(CFIN1, CFIN2)$	430
00240	161.	C		
00240	162.	C	AMPLIFICATION FACTOR CALCULATION (INTERACTION CONTRIBUTION FIRST)	470
00240	163.	C		
00241	164.		$CFIX = CFIN * SIN(ALPHA)$	480
00242	165.		$CFIY = CFIN * COS(ALPHA)$	490
00242	166.	C		
00242	167.	C	AMPLIFICATION FACTOR (MOMENTUM CONTRIBUTION)	500
00242	168.	C		
00243	169.		$R = ALPHA + EPS / 57.29582$	520
00244	170.		$CFMX = -CFMP * COS(R) + CFMN * SIN(R)$	530
00245	171.		$CFMY = CFMP * SIN(R) + CFMN * COS(R)$	540
00246	172.		$CFX = CFMX + CFIY$	550
00247	173.		$CFY = CFMY + CFIY$	560
00250	174.		$AF = (CFY * WSEC * CSTAR) * (1.0 / SMR) / (CFP * WPRI * CSTAR + CFX * WSEC)$	570

Appendix D
NON-FLOW THROUGH PEBBLE
BED HEATER PERFORMANCE

D-1

Appendix D

The performance of the non-flow through pebble bed heater described in Section 4.3 of this report is calculated by applying the first law of thermodynamics and the perfect gas equation of state. Applying the first law, one obtains:

$$\left[\begin{array}{l} \text{The decrease of stored} \\ \text{energy of CF}_4 \text{ in the tank} \end{array} \right] = \left[\begin{array}{l} \text{The stored energy of} \\ \text{the gas leaving the} \\ \text{tank} \end{array} \right] + \left[\begin{array}{l} \text{The flow work of} \\ \text{the gas leaving} \\ \text{the tank} \end{array} \right]$$

The above equation written in differential form is

$$mdu = p \nu dm$$

The specific internal energy of the CF_4 may be expressed as

$$u = .9313 p\nu$$

The energy balance becomes

$$\frac{dm}{m} = 0.9313 \frac{d(p\nu)}{p\nu}$$

or

$$\ln \frac{m_f}{m_u} = 0.9313 \ln \frac{P_f \nu_f}{P_i \nu_i}$$

where the subscripts f and i refer to the final and initial conditions in the heater, respectively. Further manipulation yields

$$\frac{m_f}{m_i} = \left(\frac{p_f}{p_i} \right)^{0.482}$$

This equation is somewhat conservative as the amount of heat energy added to the CF_4 through heat transfer from the pebbles was neglected.

A sample calculation using the above equation and the equation of state follows.

Consider:

$$p_i = 500 \text{ psia}; p_f = 300 \text{ psia};$$

and

$$m_i = 20 \text{ pounds of } \text{CF}_4$$

$$\therefore m_f = 20 \left(\frac{300}{500} \right)^{0.482} = 15.64 \text{ pounds}$$

Now for a set flow rate of say 2.5 pounds per second one would obtain a test "blow" of 2.5 seconds duration. Also since $p\nu = RT$ and $V = \nu/m_i$, one can solve for the required volume of the heater which for this case is 5.3 cubic feet.

It is emphasized that the preceding analysis is restricted to 100% CF_4 heated to 600°F . Analogous results may be obtained for other gases and other test conditions. However, the appropriate thermodynamic constants applying to the particular gas or gas mixture being considered must be used.